12-2016

Evaluation of several pre-clinical tools for identifying characteristics associated with limb bone fracture in thoroughbred racehorses

Anthony Nicholas Corsten
Purdue University

EVALUATION OF SEVERAL PRE-CLINICAL TOOLS FOR IDENTIFYING CHARACTERISTICS ASSOCIATED WITH LIMB BONE FRACTURE IN THOROUGHBRED RACEHORSES

by

Anthony N. Corsten

A Thesis

Submitted to the Faculty of Purdue University

In Partial Fulfillment of the Requirements for the degree of

Master of Science in Basic Medical Sciences

Department of Basic Medical Sciences

West Lafayette, Indiana

December 2016

THE PURDUE UNIVERSITY GRADUATE SCHOOL

STATEMENT OF THESIS APPROVAL

Dr. Russell P. Main, Chair

Department of Basic Medical Sciences

Dr. Timothy B. Lescun

Department of Veterinary Clinical Sciences

Dr. Joseph M. Wallace

Department of Biomedical Engineering

Approved by:

Dr. Laurie A. Jaeger

Head of the Departmental Graduate Program

TABLE OF CONTENTS

TABLE OF FIGURES

LIST OF ABBREVIATIONS

Abbreviation	Meaning
MC3	Third Metacarpal
SSMD	(Proximal Forelimb) Sesamoid
LB	Long Bone
BMS	Bone Material Strength
BES	Balanced Electrolytic Solution
TB	Thoroughbred
SB	Standardbred
QH	Quarter Horse
DP	Dorsal-Palmar
LM	Lateral-Medial
1^{st} ID	First Indentation Distance
TID	Total Indentation Distance
IDI	Indentation Distance Increase
CID	Creep Indentation Distance
ED	Energy Dissipated
US	Unloading Slope
LS	Loading Slope
TDD	Touchdown Distance
BMD	Bone Mineral Density
BMC	Bone Mineral Content
TRAB	Trabecular
CORT	Cortical (for Diaphysis)
SUBCORT	Cortical (for Metaphysis)
TOT	Total
$MOR_{LM,W}$	Section Modulus across the Lateral Medial Axis, Weighted

$MOR_{DP,W}$	Section Modulus across the Dorsal Palmar Axis, Weighted
$MOR_{P,W}$	Polar Section Modulus, Weighted
FWHM	Full-Width at Half-Maximum
DMD	Dorsal Metacarpal Disease

ABSTRACT

Author: Corsten, Anthony N., M.S. BMS
Institution: Purdue University.
Degree Received: Master of Science in Basic Medical Sciences, Fall 2016.
Title: Evaluation of Several Pre-Clinical Tools for Identifying Characteristics Associated with Limb Bone Fracture in Thoroughbred Racehorses
Major Professor: Dr. Russell Main, Ph.D.

Catastrophic skeletal fractures in racehorses are devastating not only to the animals, owners and trainers, but also to the perception of the sport in the public eye. The majority of these fatal accidents are unlikely to be due to chance, but are rather an end result failure from stress fractures. Stress fractures are overuse injuries resulting from an accumulation of bone tissue damage over time. Because stress fractures are pathological, it is possible that overt fractures can be predicted and prevented. In this study, third metacarpals (MC3) from 33 thoroughbred racehorse comprised of 8 non-fractured controls and 25 horses that experienced fracture of some limb bone were evaluated for correlative factors for fracture using reference point indentation (RPI; Biodent, Osteoprobe), peripheral quantitative computed tomography (pQCT) and Raman spectroscopy. As measured by RPI, fractured racehorses had reduced indentation distance of the RPI probe on the dorsal surface of the MC3, compared to controls. pQCT analysis revealed that horses that fractured long bones had lower cortical bone mineral density in the distal metaphysis than sesamoid fractured or control horses. Also in the distal metaphysis, horses that fractured their MC3s had greater trabecular and total bone mineral content, as well as greater geometric properties compared to other fracture and control groups. Raman spectroscopy showed that the lateral aspect of horses with MC3

fractures had greater mineral:matrix, carbonate:phosphate and decreased bone remodeling ratios compared to the other fractured and control groups. Several parameters between the two RPI devices were also significantly negatively correlated. This study shows that there are likely correlative factors for fracture using these three types of tools, and that future studies could lead to the development of a predictive model for fracture.

1. INTRODUCTION

1.1 The Problem of Racehorse Fractures

Catastrophic racehorse injuries on the track or in training result in euthanasia for the animal and large losses for the owners and trainers. Despite the fact that many injuries resulting in lameness can be recuperated from with rehabilitation, the high costs of treatment make it an unlikely option for most athletes not destined for use as breeding stock. According to the Equine Injury Database, in 2015 0.162% of approximately 300,000 racing starts resulted in a catastrophic injury, amounting to 484 fatalities [1], with many more injuries occur in training. By far, fractures are the most common racing or training related injury among Thoroughbred racehorses [2] and by one estimate fractures comprise as much as 86% of injuries [3]. Because of the low rate of treatment in favor of euthanasia, it is of great importance for the safety of equine athletes and jockeys to determine factors related to fracture risk to reduce fracture incidence overall.

The most common catastrophic skeletal fracture in Thoroughbreds in the USA is of the forelimb proximal sesamoid bones [3][4], though in the UK it is the third metacarpal [5]. The sesamoids are two small spheroid bones located on the distal end of the third metacarpal that are vital for the operation of the suspensory apparatus, which allows a horse to remain standing. Fractures in these bones are commonly uniaxial or biaxial, where the latter case is more difficult to operate on surgically and often requires the animal to be euthanized [6]. The second most common catastrophic fracture in the USA is the third metacarpal (MC3), particularly in the lateral distal condyle, which is

approximately three-fourths of all MC3 fractures [3][7]. In terms of relative incidence, by one estimate, 50% / 30% of race-related fractures, and 30% / 26% of training-related fractures were of the proximal sesamoid and MC3, respectively [3].

1.2 Factors Related to Overt Fractures and Stress Fractures in Racehorses

There are many factors that have been identified to be related to the incidence of catastrophic fracture. Two common racing surfaces are turf and dirt, and injuries were found to be more common in turf races [4]. The same paper also noted that the number of days since the last race was important: both too many (greater than 33) or too few (less than 13) days before the next race were implicated in greater fracture risk. A separate group found a similar result in that horses that did not train for 10 or 21 days were at higher risk for humeral and pelvic fractures, respectively [8]. Age has had conflicting contributions to fracture risk. One study showed that age was not a factor [4], several have shown that fracture risk increases with age [1][2] and another identified younger horses as sustaining fractures with greater frequency [3]. Sex has been analyzed in only a few studies, with Hernandez et al. showing that geldings experienced fractures with 1.7x the frequency of females [4].

Most racehorse related injuries are not considered to be a one-time, random event. It is true that these types of incidents do occur, but they are likely in higher impact races, such as hurdles [9]. It is much more likely that most racehorse fractures are instead pathological and are a result of accumulated bone tissue damage, known as stress fractures [5][10][11]. Stress fractures have a number of characteristics that differentiate them from “bad step” fractures. They occur in high-strain, cyclically loaded environments, where racing and training for equine athletes falls into this category [12].

Further evidence is that catastrophic fractures between horses tend to occur at the same location and plane of the bone consistently [10]. Empirical evidence for stress fractures in horses was shown in early studies with strain-gauges [12], and more recently the pathology has been directly identified using a number of modalities, such as MRI [13], nuclear scintigraphy [14] and scanning electron microscopy [15]. It is important from a prevention standpoint that overt fractures are predicated by stress fractures. A random event cannot be predicted except by probability, but stress fractures are a pathology that should have characteristic factors that can be identified prior to injury.

1.3 Introduction to Pre-Clinical Modalities

This study examines four pre-clinical modalities to assess their ability to detect factors related to fracture. **I hypothesize** that minimally or non-invasive measures of bone architecture, morphology, mechanical properties and biomolecular composition on cadaveric equine MC3's from racing populations will correlate with fracture risk in the MC3 and other long bones.

Reference point indentation (RPI) was developed to assess mechanical properties of biological tissues in vivo, including bone, as a complement to traditional mechanical tests, and includes the Biodent [16][17] and Osteoprobe [18][19]. Both the Biodent and Osteoprobe make microindentations into a tissue's surface using a small needle, making them minimally invasive and viable in a clinical setting. The Biodent is a benchtop device that is intended for *ex vivo* testing of tissues (though prior to the release of the Osteoprobe it was used for *in vivo* studies as well) while the Osteoprobe is intended for *in vivo* clinical use. The Biodent's measures have not been conclusively correlated to traditional mechanical test results [20], and the Osteoprobe has not yet been validated to

our knowledge. We intend to use the Biodent and Osteoprobe to determine microscale mechanical factors that relate to fracture risk.

Traditionally, fracture risk in humans is most commonly assessed by dual-energy x-ray absorptiometry (DEXA) scanning for bone mineral density (BMD) for the diagnosis of diseases like osteoporosis or Paget's disease [21][22][23][24]. However, it is limited in that it is unable to distinguish between cortical and trabecular contributions to total BMD, and is not able to obtain any volumetric measurements. Peripheral quantitative computed tomography (pQCT) is a modern, low-dosage alternative to DEXA. pQCT takes 3D scans of bones and as such can measure parameters related to BMD as well as bone geometry, and can also separate between cortical and trabecular tissues for BMD calculations. In humans, pQCT has been used to successfully correlate measures to risk of fracture in patients undergoing hemodialysis [25][26][27]. In horses, pQCT has been able to differentiate between trained and untrained animals [28] as well as identifying differences between a fractured and non-fractured MC3 by analyzing the distal subcondylar bone [29]. We also utilize radiographs in conjunction with pQCT to visualize bone defects or injuries that may have been missed during an autopsy.

Raman spectroscopy is a measurement technique that uses a laser light to detect inelastic scattering effects of an object to identify molecular properties. It has a broad range of usages, though more recently it has been used to assess biological materials, such as bone [30][31]. Among other things, Raman spectroscopy has the capability to assess immature bone deposits [32], determine relative mineralization of bone [33], identify regions of high bone turnover [34] and can be correlated with RPI devices and traditional mechanical tests [35]. In equine studies, Raman spectroscopy has been shown

to have the potential to differentiate between damaged and undamaged regions of bone in the MC3 [36]. Traditional Raman spectroscopy does not have the capability to penetrate surface tissues such as skin; however, newer designs using fiber optic probes, called spatially offset Raman spectroscopy (SORS) has been shown to penetrate skin to obtain bone measurements. Work has been done in vivo with humans, where the tibia was assessed, and the results have compared favorably to those in cadaveric tissues [30].

Thus, our study aims to validate the usage of these pre-clinical modalities for assessing fracture risk. The RPI tools provide us with high-level mechanical surface measures, pQCT and radiographs contribute architectural and morphological data while Raman spectroscopy can show changes in the molecular structure of the bone surface. **Our long term goal** is that parameters identified as related to fracture risk can be used in a statistical model to predict and prevent fractures from occurring in the first place.

2. METHODS

2.1 Collection and Preparation of Samples

All bone samples were collected from racehorses euthanized at the Indiana Grand racetrack in Shelbyville, IN, and obtained through an agreement with the Indiana Horse Racing Commission (IHRC) and the Indiana Animal Disease Diagnostic Laboratory (ADDL) over the course of three years (2013-16). Horses were initially assessed for cause of death on the racetrack by an IHRC veterinarian. Additionally, characteristic information for each horse (e.g., breed, age) would also be provided by the veterinarian. The euthanized horse would be transported on the day of euthanasia for morning accidents or would be kept at the racetrack prior to transport for afternoon or weekend accidents. Horses were transported via an unrefrigerated vehicle from Shelbyville, IN to West Lafayette, IN (approximately a 1h30m drive), at which point they were assessed by ADDL pathologists.

A legally-required necropsy was performed on each horse, during which time our research team collected the left and right MC3 (see Figure 1). Samples were kept with the skin as intact as possible for Osteoprobe testing. Each bone was wrapped in BES (Balanced Electrolytic Solution) soaked gauze to prevent dehydration of the samples, and placed in a plastic bag. Horses were often not transported directly following euthanasia and remained at the racetrack overnight. To mimic this, bones that were collected the day of death would be placed in the refrigerator for 24 hours. After the 24-hour refrigeration

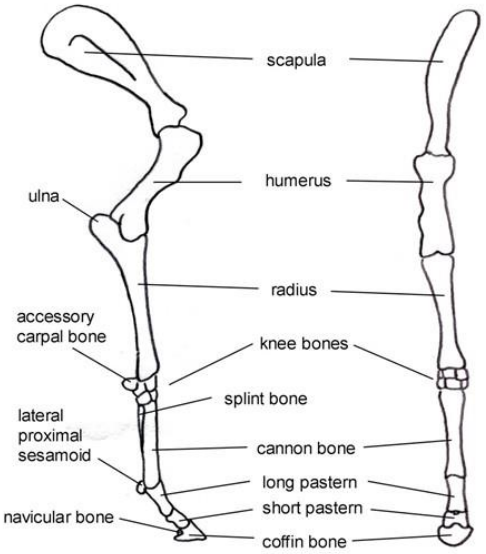

Figure 1. Equine forelimb anatomy. Notice the locations of the cannon bone (MC3) and proximal sesamoids.

period or if the bones were collected from the horse 24 hours following euthanasia, the samples were stored in a -23^{o}C freezer until tested. Typically, the time between death and freezer-storage at Purdue would be around 24-30 hours, though if a horse was euthanized before a weekend this could extend to 72 hours.

2.2 Horse Sample Demographics and Fracture Groups

Over the three years of collection, three breeds of horses were collected: thoroughbreds (TB, N = 51), Standardbreds (SB, N = 8) and Quarter Horses (QH, N = 7). Due to the significantly larger sample size of TBs, we limited the focus of our study to those horses. Within the collected TBs, there were 24 females, 8 males and 18 geldings, and one sample's gender was unknown. Horse age spanned from 2 – 7 years old at time of death. From this TB pool, a sub-sample was tested and horses were separated into statistical testing groups based on injury type (Table 1).

Table 1. Fracture Group Classifications.

Fracture Type	Male	Gelding	Female	Total	Description
MC3	1	1	2	4	Third metacarpal fracture
LB	2	3	2	7	Non-MC3 fractured long bone
SSMD	2	4	5	11	Fractured proximal forelimb sesamoid(s)
Control	2	3	5	10	No fracture
Total	7	11	14	32	

Demographics for the horses tested in each fracture group.

Alongside the fracture groups, for the purpose of statistical testing two other groups using combined demographic data were defined, shown in Table 2. The LB-combined group allowed us to examine the long-bone fracture group (LB) and the third metacarpal fracture group (MC3) compared to the sesamoid (SSMD) group or the non-fracture (Control) group. Similarly, the Fracture-combined (or Fracture) group allowed for examination of broad skeletal differences between fractured and non-fractured horses. To differentiate these from the non-combined groups, the term ‘separated’ was used when no combined groups are included in statistical comparisons.

Table 2. Combined fracture group classifications.

Classification	Description
Separated	MC3, LB, SSMD and Control all in separate statistical groups
LB-combined	MC3 and LB fractured bones in one group with SSMD and Control separated
Fracture-combined	MC3, LB and SSMD in one group with Control separated

2.3 Sample Testing Pipeline

For the purpose of assessing fracture risk, we used the reference point indentation (RPI) devices, the Biodent and Osteoprobe, as proxies of bone mechanical strength, peripheral quantitative CT (pQCT) to assess bone geometry and density and Raman spectroscopy to analyze molecular compositional characteristics of the bone at various sites throughout the MC3.

The testing pipeline was consistent to standardize the treatment of bone samples. The evening before testing (Day 0), samples were left at room temperature to thaw (approx. 16 hours). On Day 1, samples were first tested with Osteoprobe and then with the Raman microspectrometer, after which they were left in a 4^{o}C refrigerator overnight. On the morning of day 2, the sample would be tested with the Biodent and placed back into the freezer, which would limit the thawed time of a sample to less 48 hours. It has been shown that excessive freeze-thaw cycling could negatively impact Raman spectroscopy data with as few as 3 cycles [37]. Freeze-thaw cycles have also been shown to negatively impact the biomechanical properties of bone [38][39][40]. Though these papers analyzed traditional mechanical tests and not RPI, it was important to preserve data integrity by minimizing freeze-thaw cycles. Testing with pQCT could be done on frozen bones and as such did not have the strict timing windows as the rest of the pipeline. Prior to pQCT, radiographs of bones were taken to get a consistent measurement of bone length.

2.4 Testing Site Selection

The decision to test multiple locations for each modality on each bone was a direct consequence of clinical feasibility. Although we were interested in general between group and site comparisons, ultimately we were also interested in specific sites that showed differences between groups as these would be the areas to test clinically. Ideally, we would find a single site for a modality that showed significance between fracture and non-fracture horses to limit the invasiveness of any clinical testing.

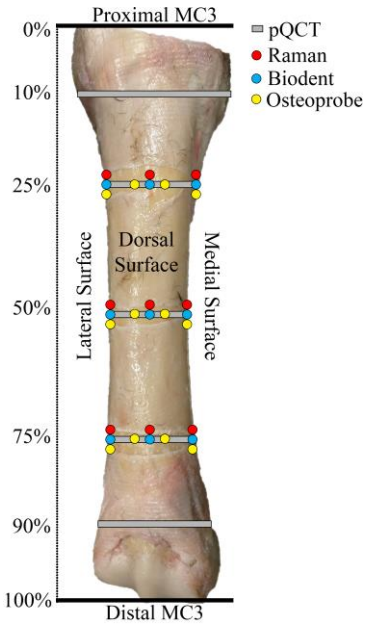

Figure 2. Tested locations for different modalities.

Raman spectroscopy and the Biodent were each tested at 3 sites along the proximal-distal axis of the limb (proximal, midshaft, distal) on the lateral, dorsal and medial aspects of the bone. The Osteoprobe was also tested at 3 sites longitudinally on the medial and lateral surfaces, but a large tendon runs along the dorsal surface of the bone and so the bone was tested dorsolaterally and dorsomedially, to mimic possible *in vivo* testing locations. pQCT measures were made along the bone's longitudinal axis, 10%, 25%, 50%, 75% and 90% of the total length. The 25%, 50% and 75% lengths correspond to the same regions that the other modalities were tested at (proximal, midshaft, distal). The 10% and 90% sites provide information on the cortical and the trabecular bone in each MC3 and slices were three times as thick at these sites. These testing locations are shown in Figure 2. By testing the same longitudinal site for our modalities, it allowed us to make statistical comparisons for parameters without worrying about varying bone composition at different sites on the bone surface.

2.5 Osteoprobe

The Osteoprobe RUO (ActiveLife Sciences, Santa Barbara, CA) was used to make indentation measurements into our samples as they would be *in vivo*. Usage of the Osteoprobe is based off of several previous publications [19][41] and adapted for use on the MC3. The Osteoprobe is a handheld RPI device for *in vivo* work while the later-mentioned Biodent is for the benchtop and is intended to be used *ex vivo*. Tests were performed twice with the device, once through the skin and once with the skin removed. After the through skin testing, the skin was removed and a small region (2-3cm across) of periosteum was scraped back from the cortical surface. Preloading was done by pressing the Osteoprobe into the cortical surface of the bone to approximately 10N to pierce the periosteum. Ten indentations at 40N were made normal to the bone surface approximately 2mm apart at each tested location. After each set of ten measurements, five control indentations were made into a block of polymethyl methylacrylate (PMMA). Tests that came out as a 'stable' (as determined by standard deviation by the Osteoprobe system) were retained while 'unstable' measurements were flagged, discarded and measurements repeated (Figure 3).

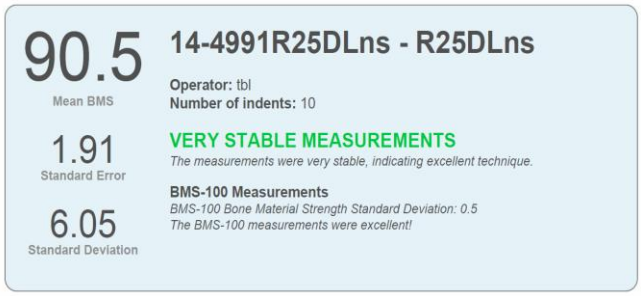

Figure 3. Typical report from the Osteoprobe. Measurements are either described as 'Very Stable', 'Stable' or 'Unstable', where the last case implies that the tests should be repeated.

Only one parameter, bone material strength index (BMSi), is measured by this instrument. Output from the Osteoprobe includes an uncorrected and corrected indentation file. The uncorrected file has all raw indentation values for bone and PMMA. The

corrected file normalizes the indentation distance into PMMA as approximately 100μm, and adjusts the indentation distances into the bone accordingly. In the corrected file, the equation for BMSi is *100 x (mean of PMMA indentation distance) / (mean of bone indentation distance)*. Thus, greater indentation distances into bone result in a lower BMSi, and vice-versa. A custom MATLAB program was used to automatically compute the BMS value from the corrected indentation distance files using the previously described equation. These were verified against the graphical report provided for each test (Figure 3).

2.6 Biodent

The Biodent (ActiveLife Sciences, Santa Barbara, CA) platform was used to test each sample using the BP2 probe. Our protocol was based on several prior publications that achieved consistent results using the device [42][35][43] and adapted for use in equine bone. Prior to testing a sample, an internal reference was made by indenting a block of PMMA with a touchdown distance (TDD) of approximately 150μm. The touchdown distance measures how far the indentation probe has to travel in order to reach the bone surface. A value that is too small or too large will often produce highly variable measurements. At each of the nine pre-determined anatomical locations on the bone, three replicate measurements were taken approximately 2mm apart. Extra measurements were taken if the output graph appeared to be erroneous, where an example of a good test is shown in Figure 4. Although relatively rare, this would occur most frequently with bones that had recently undergone significant surface remodeling and thus had a softer bone surface. Visually, this was often associated with increased surface roughness. A

preload of 5 cycles with 2N was used to ensure that the periosteum was pierced. Each individual test consisted of ten indentations normal to the cortical surface at 10N with a frequency of 2Hz. Triplicate data was acquired by moving the probe approximately 1-2mm from the initial testing site. When testing the medial and lateral sites, bar clamps (Home Depot, Model # 3706HD-4PK) were used to secure the bone on its side. Approximately every twenty minutes, the bone was sprayed with BES to prevent it from drying out.

The Biodent system automatically produced an output text file with relevant parameters calculated. These parameters were later extracted from the file for use in statistical testing, and a list of them can be found in Table 3.

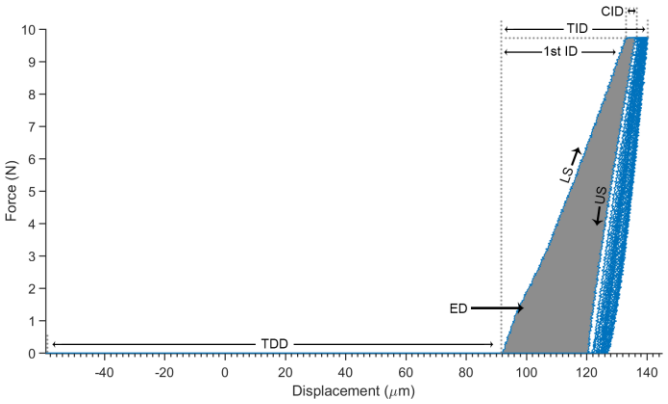

Figure 4. Example output from the Biodent machine showing the Force-Indentation curve of the indentation probe moving relative to the reference probe. Each 'loop' of on the curve is an indentation cycle, and the loops move from left to right as the bone is indented further.

Table 3. Biodent parameters of interest.

Parameter	Description
First Indentation Distance (μm) (1st ID)	First indentation distance of the probe into the bone surface
Total Indentation Distance (μm) (TID)	Total indentation distance of the probe
Indentation Distance Increase (μm) (IDI)	Difference between the first and last indentation distance including creep
Average Creep Indentation Distance (μm) (Avg. CID)	Average creep indentation distance per cycle
Average Energy Dissipated (μJ) (Avg. ED)	Average energy dissipated per cycle
Average Unloading Slope (N/μm) (Avg. US)	Average unloading slope of the Force-Indentation curve per cycle
Average Loading Slope (N/μm) (Avg. LS)	Average loading slope of the Force-Indentation curve per cycle

2.7 Raman Spectroscopy

The Horiba HR800 Raman Spectrometer (HORIBA Scientific, Atlanta, GA) was used in conjunction with a 660nm laser (Laser Quantum, Santa Clara, CA) at 75% power to obtain spectral results. A BX41 microscope (Olympus, Tokyo, Japan) and 50x objective was used to focus the laser onto the samples. The original microscope base was removed and replaced with a 6” x 5” laboratory scissor jack (Eisco Labs, India) to focus the image, as the bones were too large to fit between the original stand and the lens. The bone surface was sprayed with BES approximately every 20 minutes to prevent it from drying out.

LabSpec 5 (HORIBA Scientific, Atlanta, GA) software was used to control the laser and the spectrometer to obtain spectral readings. A darkroom was also utilized to minimize light contamination. Before testing samples, the machine was calibrated using a

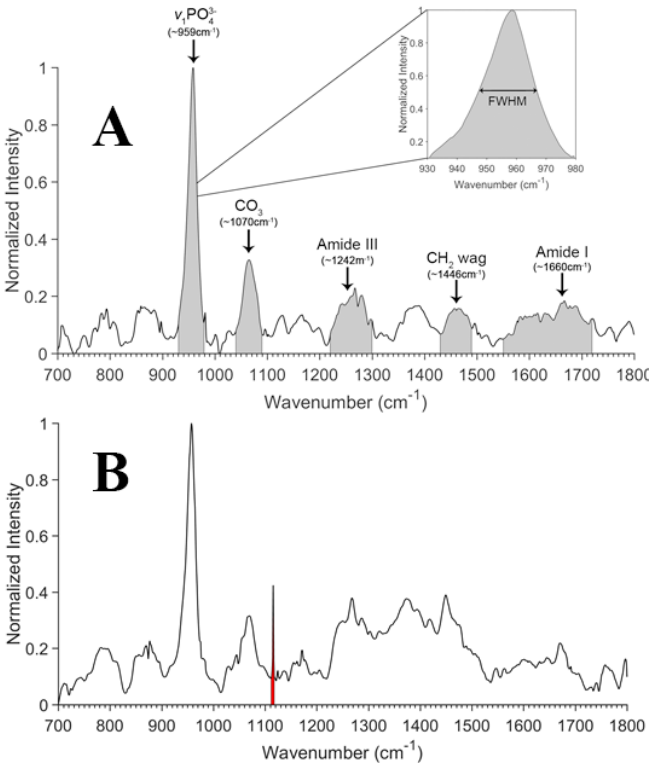

Figure 5. (A) A typical Raman shift output plot for the cortical equine MC3. The shaded areas are the Raman shift ranges belonging to each of the respective peaks. The peak value is shown in parentheses. The inset shows a representation of the full-width half max bandwidth for the phosphate peak in the figure. (B) Example of a random spike in an otherwise typical Raman spectroscopy reading, shown in red.

disc of silicon dioxide (SO_2), which has a well-resolved Raman shift peak at 520.7cm^{-1}. For data acquisition, a 20s exposure time with 5 acquisitions per spectral region between the range of 700 – 1800cm^{-1} was used. This spectral range allows for capture of a majority of the spectrum of cortical bone. The sample was moved approximately 2mm between subsequent scans to obtain triplicate measurements at each anatomical site. If spectral measurements were not visually well-resolved, then the bone surface was scraped lightly with a scalpel to remove any extant periosteum. Measurements were also repeated if significant data spiking occurred due to a variety of factors (vibrations, solar flares, random noise), as shown in Figure 5, alongside a normal spectrum. Baseline corrected (using the 'Auto' correction for consistency, which performs a linear baseline correction with 2 – 8 points, optimally determined by LabSpec) data was collected and stored in text files. These files contained the wavenumber in one column and the associated intensity values in another. Crystallinity of the $v_1 PO_4^{3-}$ phosphate peak was

computed by fitting a Gaussian curve to the data in the range of 930cm^{-1} – 980cm^{-1}. The standard form of the Gaussian function is:

$$f(x) = ae^{-\frac{(x-b)^2}{c^2}}$$

Where MATLAB was be used to find coefficients *a*, *b*, and *c* after fitting the discrete data to a Gaussian model. In the Gaussian distribution, $a = \frac{1}{\sigma\sqrt{2\pi}}$ (function magnitude), $b = \mu$ (the mean of the function) and $c = \sigma$ (the standard deviation). The full-width at half-maximum (FWHM, represented in Figure 5) value for the Gaussian function is the distance between the x-coordinates where the y-coordinate is at half of the maximum. For symmetrical Gaussian distributions, this is well-defined as $2c\sqrt{2ln2}$. A measure of relative crystallinity or mineral maturity is then computed as 1/FWHM.

Table 4. Raman spectroscopy parameters of interest.

Parameter	Description
1/FWHM of $\nu_1 PO_4^{3-}$	Crystallinity or mineral maturity of hydroxyapatite crystals
$\nu_1 PO_4^{3-}$ / Amide I	Mineral-to-matrix ratio
$\nu_1 PO_4^{3-}$ / Amide III	Mineral-to-matrix ratio
$\nu_1 PO_4^{3-}$ / CH_2 wag	Mineral-to-matrix ratio
CO_3^{2-}/ $\nu_1 PO_4^{3-}$	Carbonate substitution for phosphate
CO_3^{2-} / Amide I [34]	Remodeling / turnover rate

2.8 Radiographs

Radiographs were taken at the Purdue Veterinary Hospital by trained veterinarian technicians. Images were taken from the dorsal-palmar (DP) and lateral-medial (LM) perspectives. A 1in. diameter ball was used as a reference for scale. Images were provided via email where bone length and various cortical thicknesses were of interest.

Radiographs were also used to diagnose bone trauma that would be undetected by a surface examination. Radiographs for our four MC3 fractures from our study are shown in Figure 6.

To measure bone length, a calibration measurement was first taken on the reference ball on the radiograph to create a conversion between pixel length of the image and inches (Asteris Keystone, Asteris, Stephentown, NY). The ruler tool was then used to measure a straight line from the proximal end of the bone to the distal end. This distance was automatically converted by the program into bone length in centimeters and inches. When not using Keystone, a custom MATLAB code (MathWorks, Natick, MA) was used that could automatically determine the conversion factor using the circular Hough transform in the image processing toolbox. After that, a line could be drawn on the image by clicking two points to measure bone length in a similar manner to Keystone. This was used only in the case that Keystone files were not available (i.e., jpeg images only).

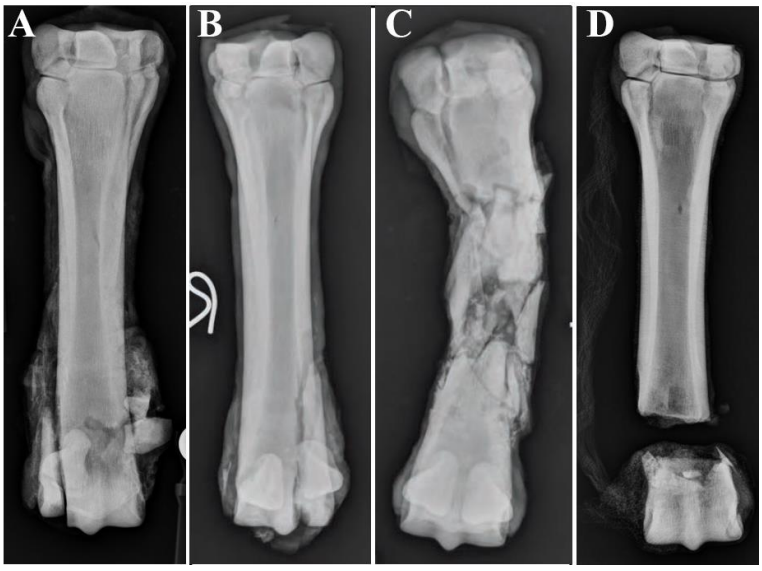

Figure 6. Radiographs of the four fractured MC3's in our pool. (A) lateral distal condyle fracture of the left MC3. (B) lateral distal condyle fracture of the right MC3. (C) comminuted midshaft fracture of the left MC3. (D) complete distal head fracture of the left MC3.

2.9 Peripheral Quantitative Computed Tomography (pQCT)

The XCT 3000 (Stratec, Birkenfield, Germany) was used for all pQCT measurements. Once per testing day, the machine was calibrated using the provided calibration samples, and tests were only conducted if the standards yielded approved results. The XCT 3000 uses a voxel size of 0.1mm x 0.1mm x 2.2mm, where 2.2mm is measured along the length of the bone. A 2.2mm thick slice was obtained at the predetermined lengths of bone (see Figure 2) by inputting length obtained from radiographs. Following data collection, a macro was used (courtesy Dan Schiferl, Bone Diagnostics Inc.) to compute desired parameters based upon a manual outline of the MC3 sections at each slice.

Table 5. Hounsfield unit density values for various materials in bone.

Material	Density (mg/cm^3)
Fat	0
Water / soft tissue	60
Cancellous bone	~700
Cortical bone	1200

Analysis for pQCT is based on user-defined thresholds that determine whether tissues of different density are counted when calculating parameters. Typically, a CT scanner uses Hounsfield units, which is a linear transformation of the attenuation coefficient to compute density (mg/cm3) and has water standardized to 0 mg/cm3. The attenuation coefficient for the XCT 3000 scanner is related to how readily a material allows x-rays to pass through, where a material that is denser has a higher attenuation coefficient. The attenuation coefficient is specific to the device (as it is related to energy output), and converted densities for the XCT3000 are provided Table 5 (courtesy Dan Schiferl, Bone Diagnostics Inc., Spring Branch, TX), which uses fat instead of water as the 0 mg/cm^3 standard.

A macro (courtesy Dan Schiferl) that uses several sub-routines with different thresholds was used to compute the values for the parameters in Table 6. All of the sub-routines use thresholding, where anything less than the threshold value is not considered in calculations. Thresholding in bone is difficult because of the partial voxel effect, where if two materials of different composition are in the same voxel, the output density will be the mean of the two. For example, the periosteal edge voxels of bone can contain cortical bone and soft tissue, so the average is estimated to be ~711mg/cm^3. All thresholds in this section were determined empirically to most accurately separate cortical and trabecular components. The Cancellous Bone Density (Calcbd) sub-routine performs two separate calculations to determine the 'Total' and 'Trabecular' measurements in Table 6. The first calculation is the 'contour-mode', which uses the previously mentioned 711mg/cm^3 density to find the outer edge of the bone surface at 10%, 25%, 50% and 75%, and 169 mg/cm^3 at 90%. Then, all voxels within this contour surface are considered for the 'Total' calculations. The second calculation is the 'peel mode', where in addition to the periosteal surface value, a second value is defined to separate the endosteal bone surface from the trabeculae. The region within this endosteal circumference is measured as 'Trabecular'. To prevent any cortical bone from contaminating the results, the circumference is reduced by 5%. At 10% and 75%, a peel density of 900mg/cm^3 is used, at 25% and 50% the threshold is 600mg/cm^3 and at 90% the threshold is 1200mg/cm^3. The region between the total and trabecular regions is designated the 'cortical + subcortical' region, because it also contains any trabecular bone and other medium not included in the trabecular calculations. A different sub-routine for Cortical Bone Density (Cortbd) was used to directly compute the cortical parameters, and a density of

710mg/cm^3 was used. Cortbd explicitly searches for voxels matching the cortical density and imputes any other voxels. Typically, Calcbd is most useful in regions that contain significant amounts of cancellous (the epiphysis and metaphysis: 10%, 75%, 90%). Cortbd is most accurate where cancellous bone is minimized (the diaphysis: 25%, 50%) (Figure 7). Cortical + subcortical measures should be used instead of the cortical measures at the metaphyses. A description of each parameter of interest can be found in Table 6.

Our sample had four fractured MC3's, so precautions were taken when making measurements at regions of fracture. For example, in our distal condylar fractures (see Figure 6) the fragmented section was secured to the rest of the bone using medical tape. When creating an outline of the bone slice for the automated macros, we confirmed that there were no missing regions of bone. In the slab fractures, an air gap was present, but this should not impact calculations except for perhaps at the edges where the partial voxel effect may exist (which would decrease BMD, though not severely due to the small surface area of the fracture compared to the slice). When testing the comminuted fracture, the midshaft regions that were destroyed were imputed.

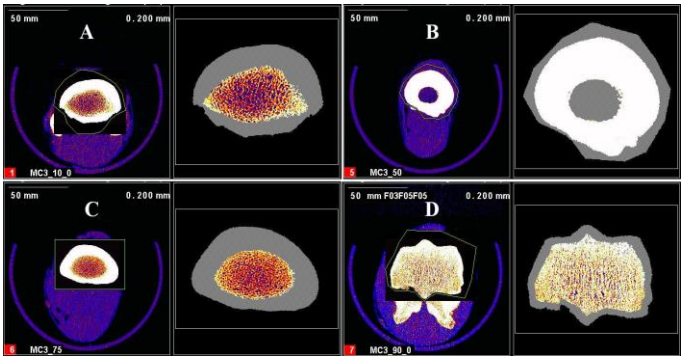

Figure 7. Typical output for Calcbd at 10%, 25%, 50%, 75% and 90% lengths. For all images, the left side represents the non-analyzed slice with an outline drawn and the right is after analysis of the outlined region using Calcbd. The grey region is the cortical + subcortical and the colored region is trabecular. (A) 10% of bone length, (B) 50% of bone length, (C) 75% of bone length (D) 90% of bone length.

Table 6. pQCT parameters of interest.

Parameter	Description
Total BMC (mg/mm) (BMC_{TOT})	Total bone mineral content
Total BMD (mg/mm^3) (BMD_{TOT})	Average volumetric bone mineral density
Total Area (mm^2) ($Area_{TOT}$)	Total cross-sectional area
Cortical-Subcortical BMC (mg/mm) ($BMC_{SUBCORT}$)	Cortical + subcortical BMC, similar measure to BMC_{CORT} for metaphyses
Cortical-Subcortical BMD (mg/mm^3) ($BMD_{SUBCORT}$)	Average cortical + subcortical volumetric bone mineral density
Cortical-Subcortical Area (mm^2) ($Area_{SUBCORT}$)	Cortical + subcortical cross-sectional area
Cortical BMC (mg/mm) (BMC_{CORT})	Cortical bone mineral content
Cortical BMD (mg/mm^3) (BMD_{CORT})	Average cortical volumetric bone mineral density
Cortical Area (mm^2) ($Area_{CORT}$)	Total cortical cross-sectional area
Trabecular BMC (mg/mm) (BMC_{TRAB})	Trabecular bone mineral content
Trabecular Density (mg/mm^3) (BMD_{TRAB})	Average trabecular bone mineral density
Trabecular Area (mm^2) ($Area_{TRAB}$)	Total trabecular cross-sectional area
Persiosteal Circumference (mm) (Perio. Circ.)	Circumference of the cortical surface
Cortical Thickness (mm) (Cort. Thk.)	Average cortical thickness
Cortical Moment of Resistance (Lateral / Medial) (mm^4) (MOR_{LM})	Resistance to lateral / medial bending in diaphysis, also called the section modulus
Cortical Moment of Resistance (Dorsal / Palmar) (Y-axis) (mm^4) (MOR_{DP})	Resistance to dorsal / palmar bending in diaphysis, also called the section modulus
Cortical Polar Moment of Resistance (mm^4) (MOR_{P})	Resistance to torsion in diaphysis, also called the section modulus
Weighted Moment of Resistance (Lateral / Medial) (mm^3) ($MOR_{LM,W}$)	Resistance to lateral / medial bending in metaphyses also called the section modulus
Weighted Moment of Resistance (Dorsal / Palmar) (mm^3) ($MOR_{DP,W}$)	Resistance to dorsal / palmar bending in metaphyses also called the section modulus
Weighted Polar Moment of Resistance (mm^3) ($MOR_{P,W}$)	Resistance to torsion in metaphyses, also called the section modulus

Abbreviation for parameters is included in parentheses.

2.10 MATLAB Data Organization

A custom MATLAB program (Mathworks, Natick, MA) was written to analyze data from each modality, outlined briefly here. Raw data from each device was initially reformatted to a standardized format (comma separated files) where columns were sorted by tested site and parameter. These files were placed into a folder for the respective testing modality. Filenames would include the accession number and the limb side (left or right). For each device, these reformatted files were then read into MATLAB, where each horse would be automatically matched with its entry in our demographical database. This included information like fracture group, age, weight and breed. Limb side was also extracted using the filename. If the horse was not found in the database due to typographical error, a notice was put into the MATLAB console and the analysis stopped.

Outliers were then removed from fracture group for each class of data using an iterative version of Grubb's test. Grubb's test checks the value with the largest deviation from the sample mean compared to the standard deviation of the sample to determine outliers [44][45]. The t-distribution is employed to compute a critical value, and the test criterion is $G = \frac{\max(Y_i - Y_{AVG})}{s}$, where the numerator computes the largest deviation and *s* is the standard deviation for the sample. The null hypothesis for this test is that an outlier does not exist, and the alternative hypothesis is that one does. If G is greater than the critical *t*-distribution value at the given α (for this paper, $\alpha = 0.001$ was used) then the null hypothesis is rejected and the value is considered an outlier. This procedure was run until the current value failed to reject the null hypothesis.

Power analysis using paired t-tests and $\beta = 0.8$ confirmed that there were no left / right differences in parameters within the sample size scope of our experimental design.

The outlier-removed data was then averaged between left and right limbs by parameter and site. Thus, each horse was only represented once even if left and right measurements were taken. If there was any missing data, then the average would only include data from a single limb. If no limb data existed at the specific site, then the site was imputed to prevent numerical errors during statistical testing. For statistical testing, data was further averaged by site, because all sites were tested in at least triplicate. Data with its associated site and demographic information was then output to an excel file that could be input into SPSS for statistical testing.

2.11 Statistical Testing

After basic descriptive statistics were computed, the MATLAB program organized data so that it could be run by SPSS 23 (IBM, Armonk, NY) syntax. A mixed-model approach was used, which is able to limit correlated error from within-subjects through the use of a random intercept, a typical issue in classic repeated measures two-way ANOVA (RMANOVA). It is also capable of handling missing data, which RMANOVA cannot as it expects each site to have an equal number of data points. Thus, the robustness of the mixed-model approach makes it ideal for our data. In this study, the horse accession number was treated as the random effect and was assigned a random intercept. Testing sites were common with all horses and were treated as a repeated fixed effect, while fracture group was treated as a normal fixed effect. P-values less than 0.05 were considered significant. A fixed-effects table was output that provided p-values for each fixed effect (Site and Group) and for the interaction effect (Site * Group). If the fixed or interaction effect was significant, then a Tukey *post-hoc* pairwise comparison

was performed, with Bonferroni corrections in the case of multiple pairwise comparisons. This procedure was repeated for each parameter of interest for each modality.

It should be noted that the sample size for Biodent and Raman spectroscopy vary slightly within group. It was determined earlier in the study (N = 6) for these two modalities that lateral and medial measures did not differentiate statistically, so past this sample size only lateral measurements were taken for these two tools.

A linear regression model was used for some comparisons to assess collinearity of parameters between Biodent and Osteoprobe. These devices are similar in nature and function, and it could serve as an internal validation of results if the linear regression yields a significant, strong correlation.

3. RESULTS

3.1 Osteoprobe

The summary of results for the Osteoprobe is available in Table 7. A total of 26 bones were tested via Osteoprobe, with sample sizes for Control, LB, MC3 and SSMD being 8, 6, 4 and 8, respectively. No significant main group effect was found for BMSi. Significant differences for the main site effect and a cross-over interaction effect of Group x Site were identified for all combinations of fracture groups. At the midshaft dorsomedial site Control (Mean ± Standard Error of the Mean, 71.62 ± 2.84) had a significantly smaller ($p = 0.009$) BMSi than the SSMD (84.00 ± 2.47) group. LB-combined comparisons between C and SSMD remained significant ($p = 0.007$) at the midshaft dorsomedial site. In the Fracture-combined comparison at the midshaft dorsomedial site, Control (71.62 ± 2.84) had a significantly lower ($p = 0.01$) BMS than Fracture-combined (79.30 ± 1.89) (Figure 8). Site factor pairwise analysis revealed that dorsomedial and dorsolateral sites largely had significantly lower BMSi than lateral or medial sites (Table 8). When the sites were averaged along the length of the bone into lateral, dorsal (including dorsolateral and dorsomedial) and medial, BMS remained significantly lower in dorsal sites (78.70 ± 1.19) than lateral (82.66 ± 1.31, $p < 0.001$) or medial (83.11 ± 1.31, $p < 0.001$) in the Fracture-combined comparison (Table 9, Figure 9).

Table 7. Summary table of mixed-model results for Biodent and Osteoprobe.

	Separated			LB-Combined			Fracture-combined		
Parameter	S	G	S*G	S	G	S*G	S	G	S*G
BMSi	**<0.001**	0.627	**0.009**	**<0.001**	0.418	**0.015**	**<0.001**	0.851	**0.010**
1st ID (µm)	**<0.001**	0.510	0.483	**<0.001**	0.448	0.219	**<0.001**	0.270	**0.020**
TID (µm)	**<0.001**	0.479	0.519	**<0.001**	0.170	0.469	**<0.001**	0.258	**0.022**
IDI (µm)	**<0.001**	0.217	0.743	**<0.001**	0.406	0.214	**<0.001**	0.246	0.364
Avg. CID (µm)	**<0.001**	0.549	0.642	**<0.001**	0.465	0.756	**<0.001**	0.364	0.337
Avg. ED (µJ)	**<0.001**	0.904	0.548	**<0.001**	0.735	0.872	**<0.001**	0.438	0.590
Avg. US (N/µm)	**<0.001**	0.937	0.488	**<0.001**	0.841	0.676	**<0.001**	0.553	0.620
Avg. LS (N/µm)	**<0.001**	0.353	0.273	**<0.001**	0.623	0.568	**<0.001**	0.944	0.499

S, G and S*G are Site, Group and Site * Group comparison results. Bolded values are significant, $p < 0.05$.

Table 8. BMSi interaction effects for fracture versus control with estimated means and standard error.

	Means ± SE			
Parameter	Proximal Lateral	Proximal Dorsolateral	Proximal Dorsomedial	Proximal Medial
BMSi (Fracture)	86.80 ± 1.28	86.15 ± 1.55	81.27 ± 1.96	85.16 ± 1.66
BMSi (Control)	87.32 ± 2.80	83.15 ± 4.06	79.56 ± 4.04	87.77 ± 1.91
	Midshaft Lateral	Midshaft Dorsolateral	**Midshaft Dorsomedial**	Midshaft Medial
BMSi (Fracture)	80.77 ± 1.71	79.47 ± 1.91	**79.30 ± 2.22**	82.60 ± 1.80
BMSi (Control)	82.82 ± 1.41	74.34 ± 4.97	**71.62 ± 5.42**	86.55 ± 1.04
	Distal Lateral	Distal Dorsolateral	Distal Dorsomedial	Distal Medial
BMSi (Fracture)	79.78 ± 1.31	74.93 ± 1.64	77.74 ± 1.90	79.8 ± 1.77
BMSi (Control)	83.81 ± 1.51	73.01 ± 3.83	74.38 ± 3.07	84.17 ± 1.79

Sites that are bolded are significant ($p < 0.05$) between Control and Fracture.

3.2 Biodent

The summary of the statistical results for the Biodent is available in Table 7. A total of 28 bones were tested via Biodent, with sample sizes for Control, LB, MC3 and SSMD being 8, 6, 4 and 10 respectively. No significant differences were found for the group main effect for any comparisons. Significant differences were detected at the site factor (Table 7) for all parameters with separated, LB-combined and Fracture-combined comparisons, where the dorsal sites were found to be typically different from lateral or medial sites. There were no differences moving from the proximal to distal end within any aspect. Sites were averaged along the length of the bone, and it was found that the dorsal site was significantly different than lateral or medial for all parameters, shown in Table 9 for all parameters and 1st ID / TID in Figure 9. All p-values for dorsal vs. lateral and dorsal vs. medial comparisons were found to be $p < 0.001$. 1st ID, TID, IDI, Avg. CID and Avg. ED were all larger at the dorsal site than lateral or medial. Avg. US and Avg. LS were significantly smaller at the dorsal site compared to lateral or medial. There were no significant differences for the Site main effect detected between lateral and medial sites with sites averaged.

With the fracture-combined comparison, a significant interaction effect for Site x Group was present for 1st ID and TID (Table 7). Pairwise analysis of the interaction showed that at the midshaft dorsal site, the Fracture-combined group had significantly lower values compared to Control horses for 1st ID (68.44 ± 2.34 and 84.57 ± 3.70) and TID (73.63 ± 2.54 and 91.21 ± 4.023) (Figure 8).

Table 9. Site main effect means for averaged aspects for reference point indentation parameters.

	Mean ± SE		
Parameter	Lateral[a]	Dorsal[b]	Medial[c]
BMSi	82.66 ± 1.31[b]	78.70 ± 1.19[a,c]	83.11 ± 1.31[b]
1st ID (µm)	50.17 ± 1.55[b]	69.10 ± 1.55[a,c]	51.87 ± 1.63[b]
TID (µm)	53.81 ± 1.69[b]	74.49 ± 1.69[a,c]	55.36 ± 1.78[b]
IDI (µm)	6.37 ± 0.27[b]	9.42 ± 0.27[a,c]	6.45 ± 0.28[b]
Avg. CID (µm)	1.41 ± 0.05[b]	2.00 ± 0.05[a,c]	1.42 ± 0.05[b]
Avg. ED (µJ)	30.20 ± 0.86[b]	42.10 ± 0.86[a,c]	31.18 ± 0.90[b]
Avg. US (N/µm)	0.75 ± 0.01[b]	0.70 ± 0.01[a,c]	0.74 ± 0.01[b]
Avg. LS (N/µm)	0.55 ± 0.01[b]	0.49 ± 0.01[a,c]	0.54 ± 0.01[b]

Superscripts indicate what sites that value was found to be significantly different from. The superscripts for that site are indicated in the table header. Averaged sites include proximal, midshaft and distal for each aspect of the bone.

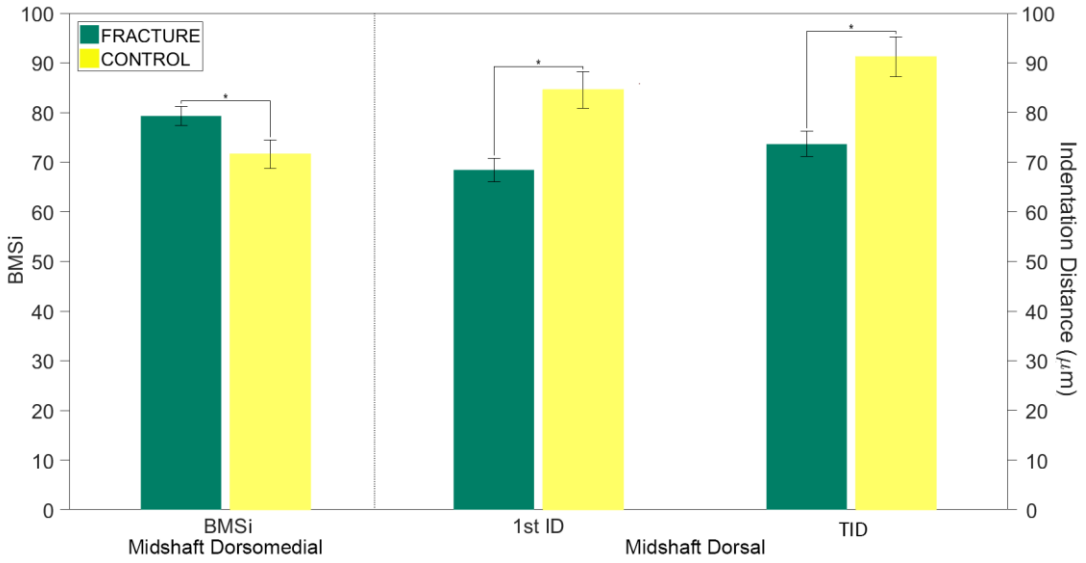

Figure 8. Three measures of reference point indentation distance with standard error bars, comparing Fracture and Control at the Group level. BMS values at the midshaft dorsomedial site were significantly greater in the Fracture group horses compared to the Control group (p = .01). The Fracture group had lower 1st ID (p = .02) and TID (p = .022) than Control at the midshaft dorsal site. This is consistent as BMS is greater in horses that achieve a lower indentation distance. BMS: N = 18 for fracture, N = 8 for control. 1st ID and IDI: N = 20 for fracture, N = 10 for control.

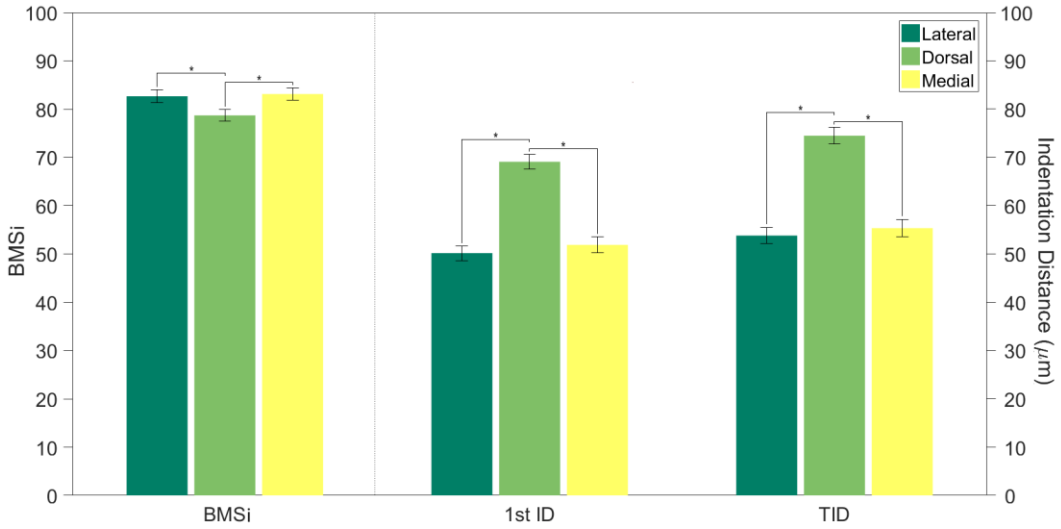

Figure 9. Three measures of reference point indentation distance with standard error bars, comparing longitudinally averaged lateral, dorsal and medial measures (including Control, LB, MC3 and SSMD). Dorsal site BMS was significantly lower than both lateral ($p < 0.001$) and medial ($p < 0.001$)sites. For the Biodent, 1st ID and TID dorsal measures were significantly greater than lateral (both $p < 0.001$) and medial (both $p < 0.001$) sites.

3.3 Linear Correlations Between Reference Point Indentation Devices

Each of the twelve sites on the Osteoprobe was paired with its equivalent site for the Biodent for linear regression. Dorsolateral and dorsomedial sites for the Osteoprobe were each paired with the dorsal site for the Biodent. Linearly regressing BMS with the Biodent parameters resulted in several significant correlations. The results are provided in Table 10. The strongest correlations were found comparing the Biodent's dorsal surface and the Osteoprobe's dorsomedial surface for 1st ID ($R^2 = 0.736$), TID ($R^2 = 0.763$), IDI ($R^2 = 0.746$), Avg. CID ($R^2 = 0.705$), Avg. ED ($R^2 = 0.464$) and Avg. US ($R^2 = 0.346$). The dorsal surfaces tended to have stronger correlations than the lateral of medial surfaces. Plots for two of the strongest correlations, 1st ID and TID vs. BMS at the midshaft dorsomedial site, are shown in Figure 10.

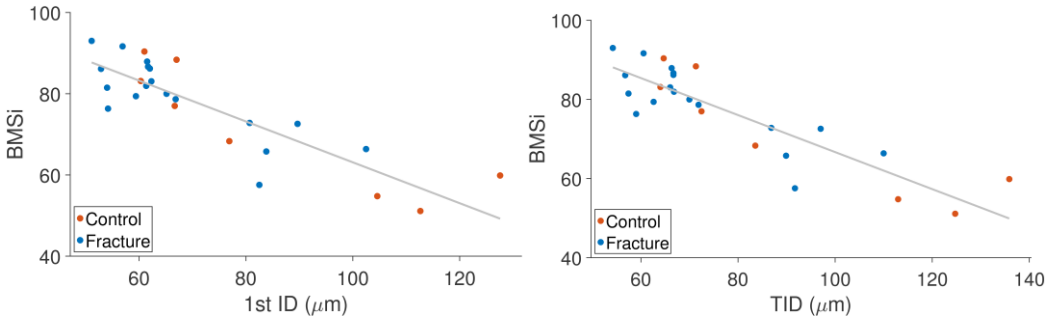

Figure 10. Correlation plots for Osteoprobe's mean BMS at the midshaft dorsomedial site versus Biodent's mean 1st ID and TID at the midshaft dorsal site for Fracture-combined and Control. The 1st ID plot had a significant ($p < 0.001$) negative correlation with an $R^2 = 0.736$. The TID comparison also yielded a significant ($p < 0.001$) negative correlation with $R^2 = 0.763$.

Table 10. Coefficients of determination comparing Osteoprobe BMSi to each Biodent parameter at all sites.

	Coefficient of Determination (R^2)						
	1st ID	TID	IDI	Avg. CID	Avg. ED	Avg. US	Avg. LS
Prox. Lat.	0.05	0.061	0.101	0.091	0.176	0.099	**0.214**
Prox. Dorsolat.	**0.539**	**0.538**	**0.442**	**0.549**	**0.485**	0.058	**0.175**
Prox. Dorsomed.	**0.713**	**0.724**	**0.661**	**0.615**	**0.581**	0.073	**0.272**
Prox. Med.	0.014	0.014	0.018	0.013	0.042	< 0.001	0.009
Mid. Lat.	0.034	0.036	0.013	0.083	0.064	0.078	0.01
Mid. Dorsolat.	**0.568**	**0.592**	**0.467**	**0.459**	**0.266**	0.012	**0.255**
Mid. Dorsomed.	**0.736**	**0.763**	**0.746**	**0.705**	**0.464**	0.041	**0.346**
Mid. Med.	**0.335**	**0.397**	**0.572**	**0.443**	**0.28**	0.171	0.139
Dist. Lat.	0.051	0.069	0.122	0.027	0.006	0.111	0.077
Dist Dorsolat.	**0.522**	**0.515**	**0.404**	**0.312**	0.087	0.048	0.004
Dist Dorsomed.	**0.643**	**0.637**	**0.516**	**0.419**	**0.157**	0.002	0.062
Dist Med.	0.151	0.178	0.176	0.017	0	0.042	0.002

Bolded correlations are significant, $p < 0.05$. All sites listed are for the Osteoprobe and are compared to the equivalent site for the Biodent. Dorsomedial and Dorsolateral measurements for the Osteoprobe are compared to Dorsal measurements for the Biodent.

3.4 Raman Spectroscopy

The full table summary of results for Raman spectroscopy analysis is available in Table 11. A total of 32 bones were tested via Raman spectroscopy, with the sample sizes for Control, LB, MC3 and SSMD being 10, 7, 4 and 11 respectively. There were no significant differences detected in the main or interaction effects with $v_1PO_4^{3-}$ (1/FWHM) crystallinity. With groups separated, the mineral-to-matrix ratios, carbonate substitution ratio and remodeling ratio were all significant for the group and site main effects. At the group level, $v_1PO_4^{3-}$ / AmideI, $v_1PO_4^{3-}$/ Amide III, $v_1PO_4^{3-}$ / CH_2 wag and CO_3^{2-} / Amide I were significantly greater in the MC3 group than the other three groups, and for CO_3^{2-}/ $v_1PO_4^{3-}$ the MC3 group was significantly lower than the SSMD group (Figure 11). Because the MC3 and LB groups were statistically different from one another in the mineral-to-matrix, carbonate substitution and bone remodeling ratios, LB-combined and Fracture-combined analyses were not done for these.

Site factor pairwise comparisons for the five significant parameters with separated groups revealed that the lateral sites (in particular at the midshaft and the proximal end) were typically different from dorsal sites and sometimes significantly different from the medial sites. Medial and dorsal sites were not found to be significantly different from one another. Within aspects comparing longitudinally, the distal lateral site was different from the midshaft lateral site for $v_1PO_4^{3-}$ / AmideI and $v_1PO_4^{3-}$ / CH_2 wag, so averaging sites longitudinally was not analyzed.

The interaction effect for separated groups was significant for all three of the mineral-to-matrix ratios (Table 11). In general, the MC3 group had larger mineral:matrix

ratios, lower carbonate substitution ratios and greater remodeling rate ratios at specific sites, but many of these comparisons were only trends and did not achieve significance.

The MC3 group had significantly greater $v_1PO_4^{3-}$ / Amide I and $v_1PO_4^{3-}$/ Amide III ratios than the other groups at all lateral sites (see Figure 12, Figure 13, Figure 14). $v_1PO_4^{3-}$ / CH_2 wag ratios, for the MC3 group were significantly greater than all other groups for the lateral sites and at the midshaft medial site, larger than LB and SSMD at the proximal medial site and larger than Control and SSMD at the proximal dorsal site.

Table 11. Summary table of mixed-model results for Raman spectroscopy.

	Separated			LB-Combined			Fracture-combined		
Parameter	S	G	S*G	S	G	S*G	S	G	S*G
Crystallinity	0.094	0.353	0.171	0.164	0.239	0.255	0.217	0.258	0.559
$v_1PO_4^{3-}$ / AmideI	**<0.001**	**0.002**	**<0.001**	-	-	-	-	-	-
CO_3^{2-}/ $v_1PO_4^{3-}$	**0.001**	**0.029**	0.086	-	-	-	-	-	-
$v_1PO_4^{3-}$/ AmideIII	**<0.001**	**0.003**	**<0.001**	-	-	-	-	-	-
$v_1PO_4^{3-}$ / CH_2wag	**<0.001**	**0.001**	**<0.001**	-	-	-	-	-	-
CO_3^{2-} / AmideI	**0.001**	**0.013**	0.064	-	-	-	-	-	-

S, G and S*G are Site, Group and Site * Group comparison results. Bolded values are significant, $p < 0.05$. A dashed line indicates that a significant difference was found between two groups intended to be averaged and further combined groups were not analyzed.

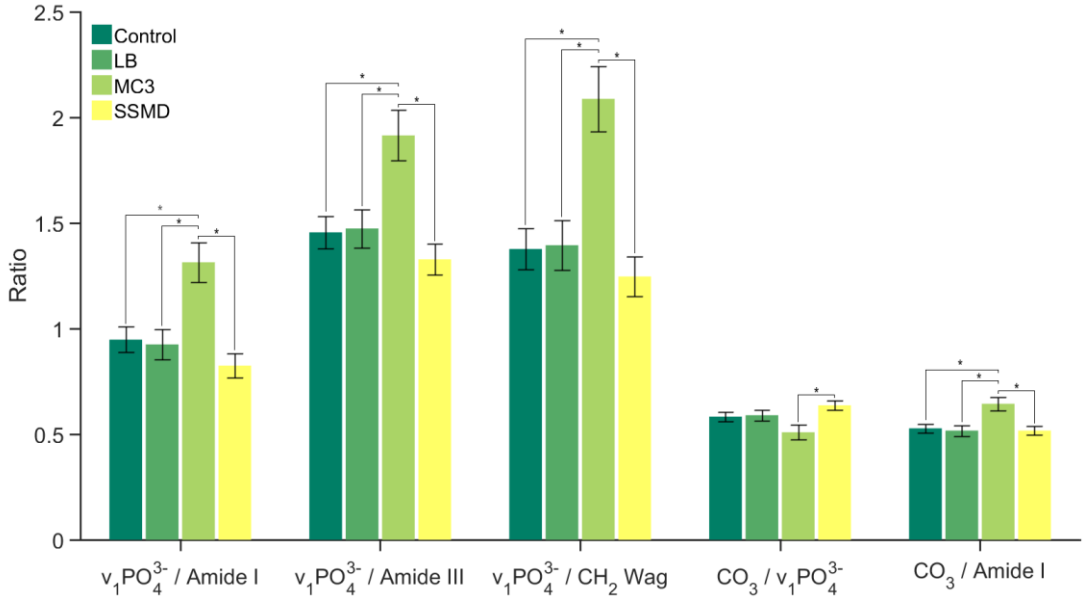

Figure 11. Significant Raman spectroscopy ratios by separated fracture group with standard error bars examining differences for the Group main effect. The MC3 fracture group (N = 4) was significantly greater in mineral:matrix measures than the Control (N = 10), LB (N = 7) or SSMD (N = 11) groups. The MC3 group was also significantly lower in carbonate substitution measures compared to the SSMD group but significantly greater in bone turnover measures than all other groups.

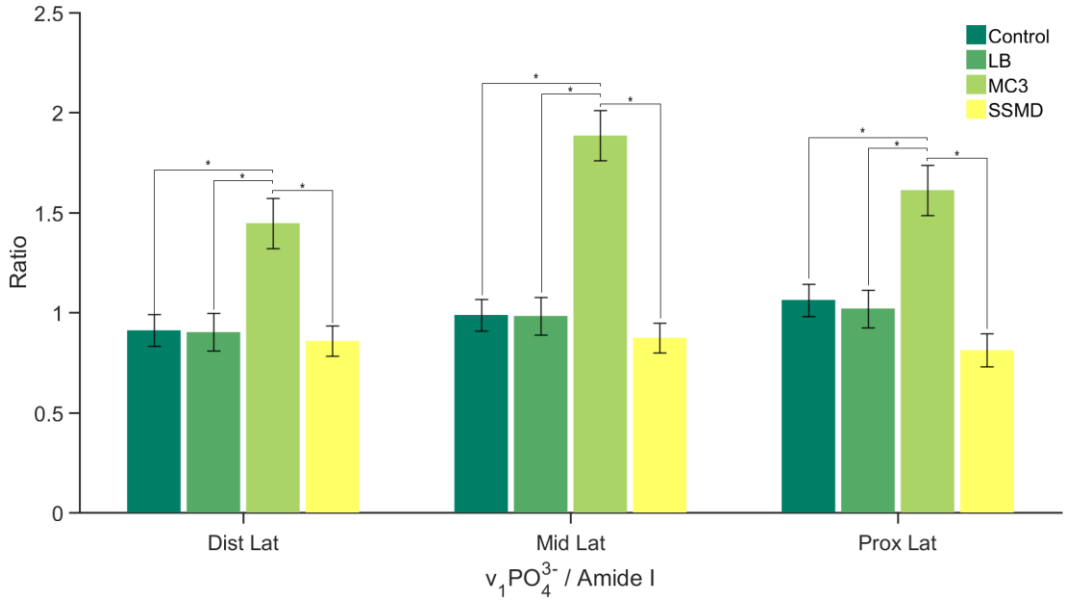

Figure 12. Statistically significant sites for the $v_1PO_4^{3-}$ / AmideI interaction effects separated by fracture group with standard error bars. In all three lateral sites, the MC3 fracture group (N=4) was significantly greater in mineral:matrix measures than the Control (N = 10), LB (N = 7) or SSMD (N = 11) groups.

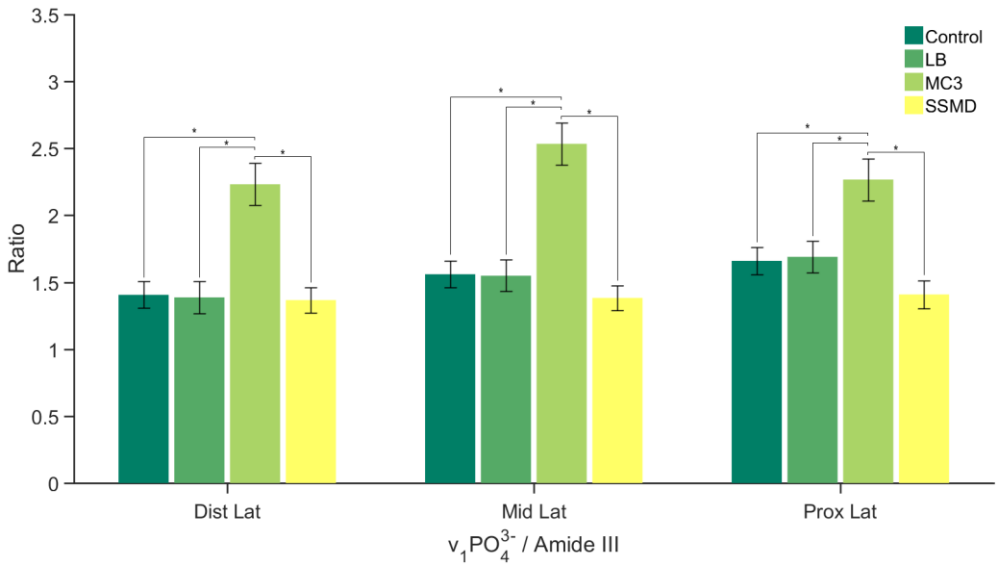

Figure 13. Statistically significant sites for the $v_1PO_4^{3-}$ / AmideIII interaction effects separated by fracture group with standard error bars. In all three lateral sites, the MC3 fracture group (N=4) was significantly greater in mineral:matrix measures than the Control (N = 10), LB (N = 7) or SSMD (N = 11) groups.

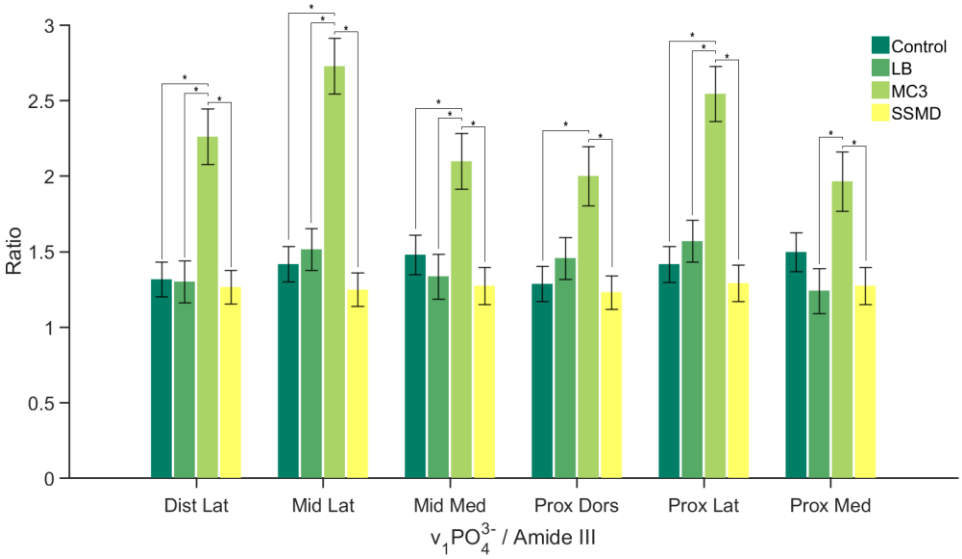

Figure 14. Statistically significant sites for the $v_1PO_4^{3-}$ / CH_2 wag interaction effects separated by fracture group with standard error bars. In all three lateral sites, the MC3 fracture group (N=4) was significantly greater in mineral:matrix measures than the Control (N = 10), LB (N = 7) or SSMD (N = 11) groups. Unlike the other two mineral:matrix measures, the MC3 group was also greater at the midshaft medial, proximal dorsal (compared to Control and SSMD) and proximal medial (compared to LB and SSMD) sites. It should be noted however that the MC3 group's mineral:matrix ratio was generally greater than all other groups at all sites, though many of these differences were not significant.

3.5 pQCT

The summary of statistical results for the pQCT is available inTable 12. A total of 33 bones were tested via pQCT, with the sample sizes for Control, LB, MC3 and SSMD being 10, 8, 4 and 11 respectively. All parameters for all comparisons were statistically significant by site, which is expected because the bone composition and geometry of the diaphysis differs from the metaphyses. For separated groups, two parameters had group level significance, BMD_{CORT} and $BMD_{SUBCORT}$. For BMD_{CORT}, LB was significantly less than SSMD ($p = 0.037$, 949.510 ± 34.43 and 978.19 ± 27.19), and for $BMD_{SUBCORT}$ the Tukey *post hoc* did not yield significant results, although the MC3 was trending significance to be less than SSMD ($p = 0.07$). Because BMD_{CORT} did not find differences between LB and MC3, they were averaged and the LB-combined comparisons were done, where a significant group difference was found again ($p = 0.015$). Pairwise analysis revealed that BMD_{CORT} for the LB-combined group was significantly less than the SSMD group ($p = 0.016$, 952.36 ± 28.63 and 978.19 ± 27.19).

All significant interactions for comparisons occurred at the 90% length, which corresponds to the distal end of the bone (Figure 2). However, several significant parameters (those obtained via Cortbd) are not valid for analysis in the metaphyses and were not analyzed here. These include: BMC_{CORT}, BMD_{CORT}, $Area_{CORT}$, MOR_{LM}, MOR_{DP} and MOR_{P}. By visual analysis, it also appears that the cortical thickness measures at the 90% site are not accurate, so they will also be excluded. For BMC_{TOT}, the MC3 fracture group (1318.2 ± 122.32) had significantly greater values than the LB ($p = 0.009$, 1117.9 ± 44.60), SSMD ($p = 0.012$, 1136.5 ± 37.30) or Control ($p = 0.001$, 1075.7 ± 45.94). BMD_{TOT} had a significant interaction effect ($p = 0.029$) for the LB-combined

comparison, but the Tukey post hoc test did not yield significant results. For $Area_{TOT}$, the MC3 fracture group (1814.6 ± 122.90) was significantly greater than LB ($p = 0.011$, 1578.7 ± 79.39), SSMD ($p < 0.001$, 1485.8 ± 43.90) or Control ($p < 0.001$, 1427.2 ± 51.35). $BMD_{SUBCORT}$ was significantly lower in the MC3 group (820.50 ± 33.21) than LB ($p = 0.002$, 916.26 ± 33.64), SSMD ($p < 0.001$, 976.68 ± 29.56) or Control ($p < 0.001$, 990.42 ± 25.93). In the same parameter, LB was also significantly less than SSMD ($p = 0.022$) and Control ($p = 0.002$). BMC_{TRAB} was significantly greater in the MC3 group (869.62 ± 64.91) compared to LB ($p < 0.001$, 654.51 ± 54.84), SSMD ($p < 0.001$, 635.98 ± 58.49) or Control ($p < 0.001$, 589.16 ± 50.60). The MC3 group (1274.8 ± 89.99) was significantly greater in $Area_{TRAB}$ compared to LB ($p = 0.008$, 1073.7 ± 69.20), SSMD ($p < 0.001$, 976.71 ± 55.32) or Control ($p < 0.001$, 937.31 ± 47.10). The LB group was also significantly greater than the Control group ($p = 0.03$) for $Area_{TRAB}$. Periosteal circumference was greater in the MC3 group (150.52 ± 5.42) than in LB ($p = 0.043$, 140.50 ± 3.58), SSMD ($p = 0.001$, 136.48 ± 2.04) or Control ($p < 0.001$, 133.7 ± 2.37). $MOR_{LM,W}$ was greater in the MC3 group (5421.9 ± 690.97) than LB ($p = 0.001$, 4028.3 ± 248.94) , SSMD ($p < 0.001$, 3969.8 ± 155.30) or Control ($p < 0.001$, 3846.7 ± 212.51). $MOR_{P,W}$ was greater in the MC3 group (11299 ± 1268.9) than Control ($p = 0.005$, 9120.6 ± 449.12).

Table 12. Summary table of mixed-model results for pQCT.

	Separated			LB-Combined			Fracture-combined		
Parameter	S	G	S*G	S	G	S*G	S	G	S*G
BMC_{TOT}	**<0.001**	0.947	**0.001**	-	-	-	-	-	-
BMD_{TOT}	**<0.001**	0.535	0.156	**<0.001**	0.367	**0.029**	-	-	-
$Area_{TOT}$	**<0.001**	0.714	**<0.001**	-	-	-	-	-	-
$BMC_{SUBCORT}$	**<0.001**	0.492	0.385	**<0.001**	0.508	0.143	**<0.001**	0.857	0.599
$BMD_{SUBCORT}$	**<0.001**	**0.045**	**<0.001**	-	-	-	-		-
$Area_{SUBCORT}$	**<0.001**	0.833	0.074	**<0.001**	0.772	0.078	**<0.001**	0.806	0.471
BMC_{TRAB}	0	0.172	**0.045**	-	-	-	-	-	-
BMD_{TRAB}	0	0.304	0.509	0	0.787	0.91	0	0.795	0.888
$Area_{TRAB}$	0	0.198	**0.013**	-	-	-	-	-	-
BMC_{CORT}	**<0.001**	0.814	**<0.001**	-	-	-	-	-	-
BMD_{CORT}	**<0.001**	**0.034**	0.262	**<0.001**	**0.015**	0.074	-	-	-
$Area_{CORT}$	**<0.001**	0.497	**<0.001**	-	-	-	-	-	-
Crt. Thk.	**<0.001**	0.679	**<0.001**	-	-	-	-	-	-
Perio. Circ.	**<0.001**	0.675	**0.001**	-	-	-	-	-	-
MOR_{LM}	**<0.001**	0.051	**<0.001**	-	-	-	-	-	-
MOR_{DP}	**<0.001**	0.263	**<0.001**	-	-	-	-	-	-
MOR_{P}	**<0.001**	0.298	**<0.001**	-	-	-	-	-	-
$MOR_{LM,W}$	**<0.001**	0.689	**<0.001**	-	-	-	-	-	-
$MOR_{DP,W}$	**<0.001**	0.662	0.392	**<0.001**	0.651	0.476	**<0.001**	0.351	0.181
$MOR_{P,W}$	**<0.001**	0.772	**0.001**	**<0.001**	0.656	0.161	**<0.001**	0.352	0.131

S, G and S*G are Site, Group and Site * Group comparison results. Bolded values are significant, $p < 0.05$. A dashed line indicates that significance between two groups intended to be averaged was found and further combined groups were not analyzed.

4. DISCUSSION

The purpose of this study was to determine if there are any correlations from several pre-clinical modalities (Raman spectroscopy, pQCT, Biodent and Osteoprobe) to increased risk of fracture. Thoroughbred racehorses have a relatively high incidence of overt fracture [2][3][4] likely due to an accumulation of fatigue damage [5][10][11]. Here, we conducted *ex vivo* tests on the MC3's of 33 thoroughbred racehorses sorted into statistical groups based on their fracture types (MC3, long bone (LB), distal sesamoid (SSMD) and non-fracture (Control)) to determine if any statistical differences existed between fracture and non-fracture groups, but also between the different fracture groups. pQCT revealed differences at the distal metaphysis (90%) for bone mineral measures and bone geometry between the MC3 group and LB, SSMD and Control groups. Analysis of RPI results showed that indentation distance measurements were different on the dorsal surface between Fracture and Control groups. Raman spectroscopy results were significantly different on the lateral surface for mineral:matrix, carbonate:phosphate and carbonate:amideI ratios between the MC3 group and LB, SSMD and Control groups. Table 13 briefly summarizes the findings from this study as compared to the Control group. Detailed information for each comparison can be found in the Results.

Table 13. Summary of significant differences compared to non-fractured horses.

Group	pQCT	Raman	Osteoprobe	Biodent
MC3	Distal metaphysis: decreased cortical BMD, increased trabecular and total BMC; increased geometric properties Distal diaphysis: increased cortical thickness	Lateral diaphysis: increased mineral:matrix (CH_2 wag also increased on dorsal and medial diaphysis). Group factor: increased carbonate substitution, decreased remodeling rate	Midshaft dorsomedial: Increased BMS	Midshaft dorsal: Decreased 1st ID, TID
LB	Distal metaphysis: decreased cortical BMD	None		
SSMD	None	None		

4.1 pQCT

Significant results for the pQCT were all found at the distal metaphysis (90%) of the MC3. Although a great number of parameters were significant, we are primarily interested in the significant differences observed in BMC_{TRAB}, BMC_{TOT} (BMC_{TRAB} + $BMC_{SUBCORT}$) and $BMD_{SUBCORT}$ as measures of mineralization, and $Area_{TRAB}$, $Area_{TOT}$, Crt. Thk., Perio. Circ., $MOR_{LM,W}$ and $MOR_{P,W}$ for the bone geometry at the distal metaphysis. The majority of the significant differences for these parameters were observed between the MC3 fracture group and the LB, SSMD and Control groups.

4.1.1 Bone Mineral Content and Bone Mineral Density

The finding that $BMD_{SUBCORT}$ was lower in the MC3 group than all other groups but BMC_{TRAB} and BMC_{TOT} were greater at the distal metaphysis is relevant to our testing population, considering that three of the four MC3 fractures in our sample occurred at the distal end of the bone. One of these involved a complete fracture proximal to the distal condyle, and two were slab fractures of the lateral distal condyle. This has also been shown in epidemiological studies, where approximately 75% of MC3 fractures were in the distal lateral condyle[3][7].

The role of BMD and BMC in fracture risk is complicated. Excessively low BMD is associated with fracture-prone bones [22], so this low $BMD_{SUBCORT}$ measure could be influencing the high prevalence of fractures at the distal condyle of the MC3. There have been a number of studies that used pQCT to assess BMD-related fracture risk in humans. One study found that in hemodialysis patients, a lower BMD_{CORT}, cortical thickness and $Area_{CORT}$ was associated with fracture but trabecular measures were not able to predict fracture risk [25]. Our results are slightly different, in that geometry is increased in our sample instead of decreased, so a different mechanism is likely involved (see section *4.1.2*). Regarding cortical BMD, other studies have shown that the cortical measures of pQCT are relevant to fracture risk while trabecular components are not [26][27]. Low BMD in humans in high loading environments has also been associated with fatigue fractures in both male and female marines in training [46][47], which is relevant to the high-impact training that racehorses endure. It was not assessed, however, if this low BMD was caused by increased porosity or low bone tissue mineralization. Regardless, these studies show that our finding of low $BMD_{SUBCORT}$ are likely to be relevant to

increased fracture risk, although unlike the hemodialysis studies we also found that a trabecular component (BMC_{TRAB}) was involved, possibly because their findings were not in the distal condyles, and not in the same animal.

Several other studies have shown that in equine bones, subcondylar cancellous bone has greater bone density [48][49] in trained horses compared to non-trained animals, assessed by CT. Another equine study using High Resolution (HR)-pQCT observed that there was increased bone volume / total volume (BV/TV) in fractured distal condyles compared to non-fractured samples. This is similar to our results, in that we saw an increase in BMC_{TOT} and BMC_{TRAB} in the distal condyles, though it does not explain why we saw a decrease in $BMD_{SUBCORT.}$

One possibility is that both low-density cortical bone and normal-density trabecular bone are being added to the distal subcondylar bone in MC3 fractured horses. This would cause the BMC_{TRAB} and BMC_{TOT} to increase (as any increased bone mass will increase BMC), but will reduce $BMD_{SUBCORT}$. The lack of significant differences between the MC3 group and other groups for BMD_{TOT} are possible if the changes in the amount of low-density cortical bone and normal density trabecular bone are similar. Thus, the large change in $BMD_{SUBCORT}$ in the MC3 fracture horses was perhaps enough to make these bones more fracture-prone compared to the other groups.

It was also found that $BMD_{SUBCORT}$ was significantly less in the LB group than the SSMD or Control groups (but greater than the MC3 group). This may indicate that horses with lower $BMD_{SUBCORT}$ are more fracture prone in the long bones in general, but a larger sample size may be useful in showing this effect. How exactly differences in BMC_{TRAB}, BMC_{TOT} and $BMD_{SUBCORT}$ affect overall bone strength, ductility and

resistance to stress fractures is not possible to assess in this study, but all are known to be critical for bone strength [50][51][52].

4.1.2 The Effect of Geometric Properties on Fracture Susceptibility

Bone geometry has been shown to be important in assessing stress fracture risk [46][47] and mechanical strength [53], where higher section moduli and cortical bone area are associated with decreased fracture risk. It has even been shown in one study in humans that section modulus is more important in determining the activity level of an individual than BMD [54].

In our study, it is shown that distal $MOR_{P,W}$ is greater in the MC3 group than the Control group and that $MOR_{LM,W}$ is greater in the MC3 group than all other groups. This is possibly contradictory to [54], as in our MC3 group, we see decreased $BMD_{SUBCORT}$ and increased section moduli and yet our animals are still more susceptible to MC3 fracture, which is likely indicative of sub-cortical remodeling. This might be explained by the fact that the human study was in fully-grown adults, and the horses in our study are not yet skeletally mature so they are still experiencing bone modeling. Thus, it may prove more fruitful to understanding the underlying reasons for fracture risk by looking at other geometric changes.

Our data shows that at the distal metaphysis (90%), $Area_{TOT}$, $Area_{TRAB}$, cortical thickness and periosteal circumference are also all increased in the MC3 group over the other groups. This could possibly indicate that the bones are larger, maybe due to adaptations to stresses or genetic predisposition, but are mechanically weaker (due to lower $BMD_{SUBCORT}$) than the other groups. The cortical thickness was also found to be significantly less in the MC3 group at the 75% length of the bone compared to the other

groups. This could lend support to the argument that MC3 fracture horses have possibly a detrimental adaptation to loading – at the 90% site, low $BMD_{SUBCORT}$ results in slab fracture prevalence because of the low density bone deposits. At the 75% location, thinner cortical shells result in complete breakage of the distal head.

4.2 Raman Spectroscopy Analysis

4.2.1 Mineral-to-Matrix Ratio & The Hypermineralization Theory

Raman spectroscopy revealed mineral:matrix in the MC3 fracture group were greater than in the LB, SSMD and Control groups. Additionally, the MC3 group was significantly lower in carbonate substitution (CO_3^{2-}/ $v_1PO_4^{3-}$) than the SSMD group (Table 11). Although $v_1PO_4^{3-}$ / Amide I is generally understood to be a valid mineral-to-matrix measure, there is still significant discussion on the validity of the other ratios used here ($v_1PO_4^{3-}$/ Amide III and $v_1PO_4^{3-}$ / CH2wag) for mineral-to-matrix measurements [31]. Because the findings for these two ratios mirror the phosphate to amide I ratio in our study, perhaps the results can add to their validity, at least in equine bones.

Observing that MC3 fractured horses have greater mineral-to-matrix ratios on the lateral surface (and the proximal dorsal, proximal medial and midshaft medial for the CH_2 wag mineral:matrix) than not only other fracture groups but also the control group is somewhat counter-intuitive, as we may expect that greater mineralization implies lower fracture risk. One possible theory is that perhaps these MC3 bones are hypermineralized on the lateral surface of the diaphysis in response to some prior stress. An excessively high mineralization is associated with increased strength at the cost of reduced ductility [22][55]. This is somewhat supported by the fact that only one of our four MC3 fractures

occurred in the midshaft, which was a comminuted fracture, while the other three occurred at the distal end of the bone in the metaphysis. Typically, a comminuted fracture occurs in excessively brittle bones, like in osteoporosis [56]. Looking at the larger population of fractures, the majority of MC3 fractures that occur are of the distal lateral condyle [3], and it is possible that this hypermineralization allows for greater propagation of slab fractures. Perhaps these MC3 fracture horses are more resistant to midshaft MC3 fracture but are more susceptible to distal condylar fractures. In support of this notion are the results of one study [36] that found that in thoroughbred racehorse MC3s, bone samples from the midshaft with higher mineral-to-matrix ratios were more resistant to breaking via four-point bending, indicating greater mechanical strength. However, it should be noted that their assessment differs in that their sample size was small (N = 3) and only one horse was known to have fractured while the cause of death of the others was unknown. Regarding the findings for CH_2 wag on the dorsal and medial surfaces, it is possible that these contribute to midshaft bone strength and would be another supporting factor in the reason that midshaft fractures are rarely observed.

4.2.2 Bone Remodeling Rate

The mineralization of bone can also be heavily affected by modeling and remodeling due to microdamage, and this remodeling is reflected in the carbonate to amide I ratio [34]. In the case of thoroughbred racehorses, stress fractures in the MC3 are very common [11][57] and the healing process results in the depositing of immature, woven bone [58]. Woven bone has a disorganized collagen matrix and is largely anisotropic [59], which decreases biomechanical strength. In our samples, visual inspection shows that most of the speculated woven bone is on the dorsal surface, and the

proposed mechanism of that is explained in detail in *4.3.1*. It is possible that we are seeing the effects of secondary mineralization of previously deposited woven bone from previous micro-trauma on the lateral surface, which is why there is no visual surface roughening. Secondary mineralization occurs after the initial immature bone undergoes primary mineralization (over several weeks, typically) which involves rapid mineralization, and matures the bone mineral over a longer timespan (months to years) [60][61]. It is uncertain why this occurs in the lateral surface and not the medial surface, though this may have to do with the curvature of the medial and lateral aspects of the bone, which could lead to greater stresses and strains on the lateral aspect. It is possible that in horses that are susceptible to MC3 fractures, racing reveals a structural weakness in the lateral aspect of the bone in young racehorses and that this is remedied through bone remodeling and modeling. This is somewhat unlikely, though, as a study by Davies [62] showed that the highest compressive strains occurred on the medial surface, followed by the dorsal and then the lateral surfaces, which is similar to what was found by Gross et al. [63]. As the MC3 group was generally greater in mineral:matrix measures, and CH_2 wag was found to be greater on the dorsal and medial surfaces, more studies will need to be done in order to determine the level of mineralization for these MC3 group horses.

Alternatively, horses that experience higher stresses on the lateral surface may be genetically predisposed to hypermineralization of the bone in that region, or perhaps in the diaphysis in general. As mentioned earlier, this remodeling may make the lateral surface more susceptible to stress fractures (particularly through stresses at the distal condyle), eventually resulting in overt fracture. Further studies comparing the curvature

and physiochemical properties of trained and non-trained equine MC3's as the animal ages will be important to understanding this possible phenomenon. Differences in these properties between trained and non-trained horses would also be useful.

4.2.3 Carbonate Substitution

Analyzing the results for carbonate substitution shows us that the MC3 group bones may be undergoing active remodeling at the lateral site compared to the other groups. Phosphate ions within the crystal lattice of hydroxyapatite are readily substituted by carbonate, and this phenomenon has been shown to increase with the age of bone tissue [30][64] much like mineralization. Thus, the carbonate to phosphate ratio gives us a strong indication of the relative age of the bone tissue. In this case, we see that the MC3 group is significantly lower in this parameter on the lateral aspect than the SSMD group and trending for LB and Control groups. This supports the idea that the lateral surface of MC3 fractured bones experienced hypermineralization when the animal was young either through a response to training or by perhaps being born with greater mineralization at this site.

4.3 Reference Point Indentation

4.3.1 Fracture Risk Analysis and Dorsal Metacarpal Disease

For the Biodent, 1st ID and TID were found to be significantly lower at the midshaft dorsal site in the Fracture group than the Control. BMS was found to be significantly higher at the midshaft dorsomedial site in Fracture group horses compared to Control. This is counterintuitive, as 1st ID and TID are single-cycle measures of indentation distance and lower measures are potentially a proxy for resistance to

microfracture [35]. We would also anticipate that a higher BMS value would correspond to microfracture resistance [65] as other groups have found. Despite these findings, we would expect that as indentation distance increases for the Biodent, the BMS should decrease at the same sites, which is what was observed in our results. This implies that these observations are likely real. Before exploring these results further, it is important to discuss the significant results between aspects of the bone.

Both RPI devices showed that the dorsal surface for many parameters was statistically different than the lateral and medial surfaces (Table 9). To our knowledge, reference point indentation has not shown this phenomenon previously, especially not in equine bone. This is possibly because many studies of RPI done on long bones *ex vivo,* 1) are not done in equine and 2) are done with machined sections of bone rather than directly on the bone surface [35][66], even when testing different aspects [43]. One study that tested whole bones with the Biodent found that posterior and anterior measurements differed; however, this study was done in mice and the medial and lateral surfaces were not tested [67].

Visually, bones that tended to have higher indentation values in the dorsal surface had surface roughening and reddening. The effect did not noticeably extend to the lateral and medial surfaces in our samples. This surface observation is possibly the result of dorsal metacarpal disease (DMD), or bucked shins, which is a well-documented pathology in the third metacarpal of thoroughbred horses around 2 years old (though horses entering training older than two are also susceptible), thought to affect up to 70% of training horses [68]. The dorsal surface of affected bones undergoes significant bone remodeling, with large amounts of woven bone being deposited [12]. The periosteum is

also typically reddened and inflamed [68]. DMD can differ in its severity between horses, and this is reflected in the symptoms presented. In addition to discomfort, by one study horses exhibiting DMD had a 12% chance of developing stress fractures in their racing career [12].

Because of the increased fracture susceptibility of DMD affected animals as well as the confounding factor it can introduce, we are interested in assessing our samples for the disease. Although there are no published studies on assessing DMD with RPI, we can use proxies for its presence, such as the difference between medial, dorsal and lateral sites mentioned previously. Additionally, it should be noted that DMD typically occurs at the dorsal and dorsomedial surfaces [68], and our significant interaction effects for Biodent and Osteoprobe were at the midshaft dorsal and midshaft dorsomedial sites, respectively. Although we do present a theory as to why non-fractured horses have lower BMS and higher indentation distances next, objectively separating DMD and non-DMD horses is a high priority to reduce confounding factors.

In light of the impact of DMD and the populations that it afflicts, there are several possible explanations for our interaction effect results. DMD typically affects younger horses, and the average age of our Fracture group is higher than the Control (4.05 and 3.5 years old, though this difference is not significant, $p = 0.222$). It is possible that the Control group horses are experiencing a stronger primary mineralization response to DMD given the age difference. This could explain why fracture groups show greater BMS and reduced indentation distances than in the Control group. It could also imply that these horses were still at high-risk for fracture, but did not fracture because they died from other causes prior. Another possibility is that Control horses and Fracture horses

differ in some sort of skeletal genetic trait. This trait would cause the DMD response to be greater, but perhaps *whole bone* strength is higher in non-fracture horses. If this is the case, then specifically for thoroughbred racehorses a *lower* dorsal measurement with RPI for BMS and *higher* measurements for 1st ID and TID may be indicative of higher fracture risk. Certainly, it would behoove us to test other long bones that may not exhibit this confounding pathology, as well as non-racehorse, non-fracture animals to see if the groups differ.

4.3.2 Comparison of Reference Point Indentation Devices

Although the Osteoprobe has been available since 2013, the only study that our team is aware of that compares these devices head-to-head showed no significant correlations between the parameters of either machine [69]. In that study, 20 whole human tibias were indented at the midshaft dorsal site with both the Biodent and Osteoprobe. The loading cycles for the Biodent were similar to the ones used by our group, where both used a 10N maximum force at 2Hz. However, Karim et al. [27] included 20 cycles while we performed only 10. Additionally, their group only tested a single site with five repetitions, while in this study 9 sites for the Biodent (or 12 with the Osteoprobe) with three repetitions were used, and the entire bone averaged for linear correlation analysis. Because of the minimal differences, the two studies should be comparable. Our team found that five parameters (1st ID, TID, IDI, Avg. CID and Avg. ED) had significant linear correlations to BMS (Table 10, Figure 10). The strongest

correlation found here (TID at $R^2 = 0.571$) was much more pronounced that the strongest correlation (1^{st} Cycle US at $R^2 = 0.194$, $p = 0.053$) found in the other study. Further studies on these conflicting results should be undertaken to discern the connection (or lack thereof) between the RPI tools.

5. CONCLUSIONS AND FUTURE DIRECTIONS

BMD and BMC measurements from the distal subcondylar MC3 obtained with the pQCT likely have predictive power for fracture in MC3 fracture horses and potentially in LB fracture horses as well. Although the exact contribution of the various tissue components of BMD and BMC (cortical, trabecular and total) to fracture-risk are unclear, there is a statistical connection between decreased BMD_{CORT}, increased BMC_{TOT} and increased BMC_{TRAB} in the distal condyle MC3 fracture group compared to other fracture and non-fracture groups. We theorize that this is due to the deposition of normal-density trabecular bone and high-porosity cortical bone, which would increase BMC_{TRAB} and because $Area_{SUBCORT}$ did not change, decrease $BMD_{SUBCORT}$. There was also an increase in geometric properties (area, sectional modulus, periosteal circumference, cortical thickness) at the distal condyle between the MC3 group and the other groups, which would increase bone strength. Thus, it is possible that although the bones in the MC3 group are larger at the distal end, they are perhaps made of weaker bone material, which causes them to be fracture prone. This may be due to a poor adaptation to mechanical stresses, where a rapid increase in geometric properties is outweighed by weak, low cortical density bone.

It was also found that the LB group had less $BMD_{SUBCORT}$ than SSMD or Control but more than the MC3 group. Thus, it will be important to assess other bones that are susceptible to fracture to see if the metaphyses in those samples also exhibit similar

phenomena as seen here, as long bones in the LB-combined group may be more susceptible to fracture in general.

Raman spectroscopy found that the lateral site of MC3 horses differed in mineral-to-matrix ratios, a bone remodeling proxy ratio and the carbonate substitution ratio compared to LB, SSMD and Control groups. The theory provided here is that the lateral site of MC3 horses experiences excessive or differentially timed adaptation as a response to early years modeling. As the horse matures, denser mineral is deposited in these early-adapted regions, possibly resulting in hypermineralization of the lateral surface of MC3-fractured bones. This would make them possibly more resistant to midshaft fractures, but the brittleness associated with higher mineralization may cause distal lateral condyle slab fractures to propagate more readily.

The severity or diagnosis of dorsal metacarpal disease was not directly assessed in our study, however indentation measurements for the Biodent were increased on the dorsal surface compared to the medial or lateral, and BMS values for the Osteoprobe were decreased in the same sites. As the pathology of DMD includes increased woven bone deposition, it is likely that we are indenting immature bone which either microfractures more easily or is simply pushed out of the way during indentation. This opens the possibility for RPI to be used in the detection of DMD in the standing horse *in vivo*. There still remains the need to directly confirm the presence of DMD, which can be done with future histology studies on our samples.

The impact of suspected DMD made it difficult to assess the connection between RPI and fracture risk, as Control horses had lower BMS and higher 1st ID and TID compared to horses that sustained a fracture, when one might expect the opposite. One

theory is that Control horses are on average, younger, and are therefore still experiencing the bone modeling effects of DMD more severely, which would lead to less mineralized cortical bone. The fractured group bones may have a more mature DMD response that includes increased mineralization. This would lead to higher indentation distances in the control group over the fracture group, but perhaps the risk of overt fracture due to stress fractures associated with DMD do not peak until the disease progresses further. It is also possible that the Control group's chance of fracture was very high at the time of death, but that they may have died from other causes before they sustained a skeletal injury. Another theory is that a genetic trait in Control horses associates with more severe DMD but also a greater overall skeletal bone strength compared to horses that sustained a fracture. Regardless of which of these theories could potentially be correct, RPI has shown its capability in indirectly measuring for fracture risk, by assessing the remodeling impact of DMD. This will need to be explored further once DMD horses have been properly identified and testing groups separated. This may yield results related not only to DMD diagnosis but also for elucidating potential differences in fracture risk between horses that fracture with and without DMD.

We have shown here that the Osteoprobe and the Biodent are likely measuring similar phenomena, as several of the Biodent's parameters correlate significantly with the Osteoprobe's BMS. This is despite the fact that the force generation rate and total force of each device is very different [20]. This information could serve as cross-validation for parameters in each device, particularly when doing a combination of *in vivo* and *ex vivo* work.

These four pre-clinical devices undoubtedly have potential in assessing fracture risk *in vivo*. Their non-invasive nature makes them ideally suited for work in the standing horse, and with further validation the tools could likely be used in human athletes and soldiers for assessing stress fracture risk. This validation must include comparison of *in vivo* measures in the Osteoprobe, pQCT and Raman spectrometer to *ex vivo* data presented here. In the longer term, a logistic regression model could be used to not only incorporate factors identified as correlating with factor here, but also covariates like age, sex and weight could be included to assess their impact.

REFERENCES

[1] Anonymous, “Supplemental Tables of Equine Injury Database Statistics for Thoroughbreds,” 2016. Online access available at http://jockeyclub.com/pdfs/eid_7_year_tables.pdf

[2] H. O. Mohammed, T. Hill, and J. Lowe, “Risk factors associated with injuries in thoroughbred horses.,” *Equine Vet. J.*, vol. 23, no. 6, pp. 445–8, 1991.

[3] B. J. Johnson *et al.*, “Causes of death in racehorses over a 2 year period.,” *Equine Vet. J.*, vol. 26, no. 4, pp. 327–330, 1994.

[4] J. Hernandez, D. L. Hawkins, and M. C. Scollay, “Race-start characteristics and risk of catastrophic musculoskeletal injury in Thoroughbred racehorses.,” *J. Am. Vet. Med. Assoc.*, vol. 218, no. 1, pp. 83–6, 2001.

[5] T. D. H. Parkin *et al.*, “Catastrophic fracture of the lateral condyle of the third metacarpus/metatarsus in UK racehorses - Fracture descriptions and pre-existing pathology,” *Vet. J.*, vol. 171, no. 1, pp. 157–165, 2006.

[6] T. D. H. Parkin *et al.*, “Risk of fatal distal limb fractures among Thoroughbreds involved in the five types of racing in the United Kingdom.,” *Vet. Rec.*, vol. 154, no. 16, pp. 493–497, 2004.

[7] J. G. Peloso, G. D. Mundy, and N. D. Cohen, “Prevalence of, and factors associated with, musculoskeletal racing injuries of thoroughbreds.,” *J. Am. Vet. Med. Assoc.*, vol. 204, no. 4, pp. 620–6, Feb. 1994.

[8] T. K. Carrier *et al.*, “Association between long periods without high-speed workouts and risk of complete humeral or pelvic fracture in thoroughbred racehorses: 54 cases (1991-1994).,” *J. Am. Vet. Med. Assoc.*, vol. 212, no. 10, pp. 1582–7, May 1998.

[9] S. L. McKee, “An update on racing fatalities in the UK,” *Equine Vet. Educ.*, vol. 7, no. 4, pp. 202–204, Aug. 1995.

[10] C. M. Riggs, “Fractures - A preventable hazard of racing thoroughbreds?,” *Vet. J.*, vol. 163, no. 1, pp. 19–29, 2002.

[11] R. B. Martin, V. A. Gibson, S. M. Stover, J. C. Gibeling, and L. V. Griffin, “Residual strength of equine bone is not reduced by intense fatigue loading: Implications for stress fracture,” *J. Biomech.*, vol. 30, no. 2, pp. 109–114, 1997.

[12] D. M. Nunamaker, D. M. Butterweck, and M. T. Provost, “Fatigue fractures in thoroughbred racehorses: relationships with age, peak bone strain, and training.,” *J. Orthop. Res.*, vol. 8, no. 4, pp. 604–611, 1990.

[13] F. Audigié *et al.*, “Magnetic resonance imaging for the diagnosis of stress fractures in a horse,” *Vet. Radiol. Ultrasound*, vol. 44, no. 4, pp. 438–442, 2002.

[14] A. Valdés-martínez *et al.*, “Quantitative analysis of scintigraphic findings in tibial stress fractures inThoroughbred racehorses,” vol. 69, no. 7, pp. 1–5, 2008.

[15] M. W. Stepnik *et al.*, “Scanning electron microscopic examination of third metacarpal/third metatarsal bone failure surfaces in Thoroughbred racehorses with condylar fracture,” *Vet. Surg.*, vol. 33, no. 1, pp. 2–10, 2004.

[16] P. Hansma *et al.*, “The tissue diagnostic instrument,” *Rev. Sci. Instrum.*, vol. 80, no. 5, pp. 1–6, 2009.

[17] A. Diez-Perez *et al.*, “Microindentation for in vivo measurement of bone tissue mechanical properties in humans,” *J. Bone Miner. Res.*, vol. 25, no. 8, pp. 1877–1885, 2010.

[18] E. Torres-Del-Pliego, L. Vilaplana, R. Güerri-Fernández, and A. Diez-Pérez, “Measuring bone quality,” *Curr. Rheumatol. Rep.*, vol. 15, no. 11, 2013.

[19] C. Randall *et al.*, “Applications of a New Handheld Reference Point Indentation Instrument Measuring Bone Material Strength.,” *J. Med. Device.*, vol. 7, no. 4, pp. 410051–410056, 2013.

[20] M. R. Allen, E. M. B. McNerny, J. M. Organ, and J. M. Wallace, “True gold or pyrite: A review of reference point indentation for assessing bone mechanical properties in vivo,” *J. Bone Miner. Res.*, vol. 30, no. 9, pp. 1539–1550, 2015.

[21] T. J. Aspray, A. Prentice, T. J. Cole, Y. Sawo, J. Reeve, and R. M. Francis, “Low bone mineral content is common but osteoporotic fractures are rare in elderly rural Gambian women.,” *J. bone Miner. Res.*, vol. 11, no. 7, pp. 1019–25, 1996.

[22] C. L. Gregson, S. A. Hardcastle, C. Cooper, and J. H. Tobias, “Friend or foe: High bone mineral density on routine bone density scanning, a review of causes and management,” *Rheumatol. (United Kingdom)*, vol. 52, no. 6, pp. 968–985, 2013.

[23] B. L. Riggs, H. W. Wahner, W. L. Dunn, R. B. Mazess, K. P. Offord, and L. J. Melton, “Differential changes in bone mineral density of the appendicular and axial skeleton with aging. Relationship to spinal osteoporosis,” *J. Clin. Invest.*, vol. 67, no. 2, pp. 328–335, 1981.

[24] H. K. Genant *et al.*, “Noninvasive assessment of bone mineral and structure: state of the art.,” *J. Bone Miner. Res.*, vol. 11, no. 6, pp. 707–730, 1996.

[25] S. A. Jamal, J. Gilbert, C. Gordon, and D. C. Bauer, “Cortical pQCT measures are associated with fractures in dialysis patients.,” *J Bone Min. Res*, vol. 21, no. 4, pp. 543–8, 2006.

[26] C. R. Russo, G. Taccetti, P. Caneva, A. Mannarino, P. Maranghi, and M. Ricca, “Volumetric Bone Density and Geometry Assessed by Peripheral Quantitative Computed Tomography in Uremic Patients on Maintenance Hemodialysis,” *Osteoporos. Int.*, pp. 443–448, 1998.

[27] K. Hasegawa, Y. Hasegawa, and A. Nagano, “Estimation of bone mineral density and architectural parameters of the distal radius in hemodialysis patients using peripheral quantitative computed tomography,” *J. Biomech.*, vol. 37, no. 5, pp. 751–756, 2004.

[28] E. C. Firth and C. W. Rogers, “Musculoskeletal responses of 2-year-old Thoroughbred horses to early training. 6. Bone parameters in the third metacarpal and third metatarsal bones.,” *N. Z. Vet. J.*, vol. 53, no. 6, pp. 377–383, 2005.

[29] R. C. Whitton *et al.*, “Third metacarpal condylar fatigue fractures in equine athletes occur within previously modelled subchondral bone,” *Bone*, vol. 47, no. 4, pp. 826–831, 2010.

[30] G. S. Mandair and M. D. Morris, “Contributions of Raman spectroscopy to the understanding of bone strength.,” *Bonekey Rep.*, vol. 4, no. August 2014, p. 620, 2015.

[31] M. D. Morris and G. S. Mandair, “Raman assessment of bone quality,” *Clin. Orthop. Relat. Res.*, vol. 469, no. 8, pp. 2160–2169, 2011.

[32] M. D. Morris, C. P. Tarnowski, J. L. Dreier, and M. A. Ignelzi, “Raman Microscopy of De Novo Woven Bone Tissue,” vol. 4254, pp. 90–96, 2001.

[33] D. H. Kohn, N. D. Sahar, J. M. Wallace, K. Golcuk, and M. D. Morris, “Exercise alters mineral and matrix composition in the absence of adding new bone,” *Cells Tissues Organs*, vol. 189, no. 1–4, pp. 33–37, 2008.

[34] H. Isaksson *et al.*, “Infrared spectroscopy indicates altered bone turnover and remodeling activity in renal osteodystrophy,” *J. Bone Miner. Res.*, vol. 25, no. 6, pp. 1360–1366, 2010.

[35] M. A. Hammond, M. A. Gallant, D. B. Burr, and J. M. Wallace, “Nanoscale changes in collagen are reflected in physical and mechanical properties of bone at the microscale in diabetic rats,” *Bone*, vol. 60, pp. 26–32, 2013.

[36] K. A. Dooley, J. McCormack, D. P. Fyhrie, and M. D. Morris, “Stress mapping of undamaged, strained, and failed regions of bone using Raman spectroscopy,” *J. Biomed. Opt.*, vol. 14, no. 4, p. 44018, 2009.

[37] J.-D. P. McElderry, M. R. Kole, and M. D. Morris, “Repeated freeze-thawing of bone tissue affects Raman bone quality measurements.,” *J. Biomed. Opt.*, vol. 16, no. 7, p. 71407, 2011.

[38] M. Hongo *et al.*, “Effect of multiple freeze-thaw cycles on intervertebral dynamic motion characteristics in the porcine lumbar spine,” *J. Biomech.*, vol. 41, no. 4, pp. 916–920, 2008.

[39] J. S. Kang and N. H. Kim, “The biomechanical properties of deep freezing and freeze drying bones and their biomechanical changes after in-vivo allograft.,” *Yonsei Medical Journal*, vol. 36, no. 4. pp. 332–335, 1995.

[40] R. R. Pelker, G. E. Friedlaender, T. C. Markham, M. M. Panjabi, and C. J. Moen, “Effects of freezing and freeze-drying on the biomechanical properties of rat bone,” *J. Orthop. Res.*, vol. 1, no. 4, pp. 405–411, 1983.

[41] D. Bridges, C. Randall, and P. K. Hansma, “A new device for performing reference point indentation without a reference probe,” *Rev. Sci. Instrum.*, vol. 83, no. 4, pp. 1–8, 2012.

[42] M. A. Gallant, D. M. Brown, J. M. Organ, M. R. Allen, and D. B. Burr, “Reference-point indentation correlates with bone toughness assessed using whole-bone traditional mechanical testing,” *Bone*, vol. 53, no. 1, pp. 301–305, 2013.

[43] T. Jenkins *et al.*, “Variability in reference point microindentation and recommendations for testing cortical bone: Maximum load, sample orientation, mode of use, sample preparation and measurement spacing,” *J. Mech. Behav. Biomed. Mater.*, vol. 42, pp. 311–324, 2015.

[44] F. E. Grubbs, “Procedures for Detecting Outlying Observations in Samples,” *Technometrics*, vol. 11, no. 1, pp. 1–21, 1969.

[45] W. H. Lawton and E. A. Sylvestre, “American Society for Quality Self Modeling Curve Resolution American Society for Quality Stable URL : http://www.jstor.org/stable/1267173 Linked references are available on JSTOR for this article :,” vol. 13, no. 3, pp. 617–633, 2016.

[46] T. J. Beck *et al.*, “Dual-energy X-ray absorptiometry derived structural geometry for stress fracture prediction in male U.S. Marine Corps recruits.,” *J. Bone Miner. Res.*, vol. 11, no. 5, pp. 645–653, 1996.

[47] T. J. Beck, C. B. Ruff, R. A. Shaffer, K. Betsinger, D. W. Trone, and S. K. Brodine, “Stress fracture in military recruits: Gender differences in muscle and bone susceptibility factors,” *Bone*, vol. 27, no. 3, pp. 437–444, 2000.

[48] C. M. Riggs, G. H. Whitehouse, and A. Boyde, “Structural variation of the distal condyles of the thirdmetacarpal and third metatarsal bones in the horse.,” *Equine Vet. J.*, vol. 31, no. 2, pp. 140–148, 1999.

[49] C. E. Kawcak, C. W. McIlwraith, R. W. Norrdin, R. D. Park, and P. S. Steyn, “Clinical effects of exercise on subchondral bone of carpal and metacarpophalangeal joints in horses,” *Am. J. Vet. Res.*, vol. 61, no. 10, pp. 1252–1258, 2000.

[50] J. a Spadaro, F. W. Werner, R. a Brenner, M. D. Fortino, L. a Fay, and W. T. Edwards, “Cortical and trabecular bone contribute strength to the osteopenic distal radius.,” *J. Orthop. Res.*, vol. 12, no. 2, pp. 211–8, 1994.

[51] M. M. Barak, S. Weiner, and R. Shahar, “The contribution of trabecular bone to the stiffness and strength of rat lumbar vertebrae,” *Spine (Phila. Pa. 1976).*, vol. 35, no. 22, pp. E1153-9, 2010.

[52] G. Iolascon, R. Napolano, M. Gioia, A. Moretti, I. Riccio, and F. Gimigliano, “The contribution of cortical and trabecular tissues to bone strength: Insights from denosumab studies,” *Clin. Cases Miner. Bone Metab.*, vol. 10, no. 1, pp. 47–51, 2013.

[53] M. C. H. Van der Meulen, K. J. Jepsen, and B. Miki, “Understanding bone strength: Size isn’t everything,” *Bone*, vol. 29, no. 2, pp. 101–104, 2001.

[54] S. Kaptoge *et al.*, “Hip section modulus, a measure of bending resistance, is more strongly related to reported physical activity than BMD,” *Osteoporos. Int.*, vol. 14, no. 11, pp. 941–949, 2003.

[55] H. Follet, G. Boivin, C. Rumelhart, and P. J. Meunier, “The degree of mineralization is a determinant of bone strength: A study on human calcanei,” *Bone*, vol. 34, no. 5, pp. 783–789, 2004.

[56] K. Stoffel, S. Cunneen, R. Morgan, R. Nicholls, and G. Stachowiak, “Comparative stability of perpendicular versus parallel double-locking plating systems in osteoporotic comminuted distal humerus fractures,” *J. Orthop. Res.*, vol. 26, no. 6, pp. 778–784, 2008.

[57] C. B. O´Sullivan and J. M. Lumsden, “Case Report Distal third metacarpal bone palmar cortical stress fractures in four Thoroughbred racehorses,” *Equine Vet. Educ.*, vol. 14, no. 2, pp. 70–75, 2002.

[58] B. A. Uthgenannt, M. H. Kramer, J. A. Hwu, B. Wopenka, and M. J. Silva, “Skeletal self-repair: stress fracture healing by rapid formation and densification of woven bone.,” *J. Bone Miner. Res.*, vol. 22, no. 10, pp. 1548–56, 2007.

[59] X. Su, K. Sun, F. Z. Cui, and W. J. Landis, “Organization of apatite crystals in human woven bone,” *Bone*, vol. 32, no. 2, pp. 150–162, 2003.

[60] D. B. Burr and M. R. Allen, *Basic and Applied Bone Biology*. 2014.

[61] Y. Bala, D. Farlay, P. D. Delmas, P. J. Meunier, and G. Boivin, “Time sequence of secondary mineralization and microhardness in cortical and cancellous bone from ewes,” *Bone*, vol. 46, no. 4, pp. 1204–1212, 2010.

[62] H. M. S. Davies, “The timing and distribution of strains around the surface of the midshaft of the third metacarpal bone during treadmill exercise in one Thoroughbred racehorse,” *Aust. Vet. J.*, vol. 83, no. 3, pp. 157–162, 2005.

[63] T. . Gross, K. . McLeod, and C. T. Rubin, “Characterizing bone strain distributions in vivo using three triple rosette strain gages,” *J. Biomech.*, vol. 25, no. 38, pp. 1320–1323, 2001.

[64] O. Akkus, F. Adar, and M. B. Schaffler, “Age-related changes in physicochemical properties of mineral crystals are related to impaired mechanical function of cortical bone,” *Bone*, vol. 34, no. 3, pp. 443–453, 2004.

[65] T. B. Lescun, K. Hoffseth, H. T. Yang, P. K. Hansma, H. S. Kopeikin, and S. Chandrasekar, “Effect of various testing conditions on results for a handheld reference point indentation instrument in horses,” vol. 77, no. 1, 2016.

[66] M. Granke, A. Coulmier, S. Uppuganti, J. A. Gaddy, M. D. Does, and J. S. Nyman, “Insights into reference point indentation involving human cortical bone: Sensitivity to tissue anisotropy and mechanical behavior,” *J. Mech. Behav. Biomed. Mater.*, vol. 37, pp. 174–185, 2014.

[67] A. Carriero, J. L. Bruse, K. J. Oldknow, J. L. Millán, C. Farquharson, and S. J. Shefelbine, “Reference point indentation is not indicative of whole mouse bone measures of stress intensity fracture toughness,” *Bone*, vol. 69, pp. 174–179, 2014.

[68] D. M. Nunamaker, “On bucked shins,” *AAEP Proc.*, vol. 48, pp. 76–89, 2002.

[69] L. Karim, M. Van Vliet, and M. L. Bouxsein, “Comparison of cyclic and impact-based reference point indentation measurements in human cadaveric tibia.,” *Bone*, 2015.

APPENDIX

Demographics for Horses in Current Study

Table 14. Information pertaining to horses used in this study.

Horse ID	Sex	Age (yrs)	Fx Group	Biodent	Osteo-probe	Raman	pQCT
A13-13503	M	3	Control	Both	Both	Both	Both
A14-0419	F	3	Control	Both	Both	Both	Both
A14-14702	F	5	Control	Both	Both	Both	Both
A14-15808	F	4	Control	Both	Both	Both	Both
A15-1432	Geld	5	Control	-	-	R	R
A15-2920	F	3	Control	L	L	L	L
A15-4789	F	2	Control	Both	Both	Both	Both
A16-1177	Geld	4	Control	Both	L	Both	Both
A16-2118	Geld	4	Control	-	-	Both	Both
A16-2293	M	2	Control	Both	L	Both	Both
A14-1356	F	2	LB	Both	Both	Both	Both
A14-15954	Geld	5	LB	Both	Both	Both	Both
A14-1818	F	3	LB	Both	Both	Both	Both
A14-4992	Geld	5	LB	R	R	Both	R
A14-5202	F	3	LB	-	-	-	Both
A15-14441	Geld	3	LB	R	R	Both	Both
A15-4869	M	4	LB	Both	R	Both	Both
A15-5258	M	3	LB	-	-	L	L
A14-14505	Geld	5	MC3	Both	R	Both	Both
A14-5118	F	2	MC3	Both	Both	Both	Both
A15-4375	F	2	MC3	Both	Both	Both	Both
A15-4790	M	4	MC3	Both	R	Both	Both
A13-13148	F	3	SSMD	Both	-	Both	Both
A14-0498	F	5	SSMD	Both	Both	Both	Both

A14-0735	M	5	SSMD	Both	Both	Both	Both
A14-14416	M	4	SSMD	Both	Both	Both	Both
A14-1972	Geld	4	SSMD	Both	Both	Both	R
A14-3323	M	5	SSMD	Both	Both	Both	Both
A14-4991	F	4	SSMD	Both	Both	Both	Both
A15-14775	Geld	7	SSMD	-	-	Both	Both
A16-1925	F	5	SSMD	Both	-	Both	Both
A16-2635	Geld	4	SSMD	Both	Both	Both	Both
A16-9	F	6	SSMD	Both	Both	Both	Both

Tests completed only unilaterally are indicated by L or R, and bilaterally with 'Both'.

Biodent Protocol

Materials:

- Periosteal elevator
- Scalpel
- Bone sample (thawed)
- BES (in squirt bottle)
- The correct type of probes (BP1, BP2 etc.)
- Biodent computer and associated scale / probe holder
- C-clamps (1 or 2)
- Instrument tray for holding sample

- Paper towels (3 or 4)
- PMMA block
- Gauze

Procedure:

Preparation Stage

1) Thaw bone overnight or until completely thawed (if bone is thawed skip this step)
2) Wet paper towels and fold in-half twice (just dampened) – these will be used to prop the distal end of the bone, which serves two purposes. One, it provides friction to prevent the bone from sliding in the tray, and two, the distal end is slightly sloped, so it makes the entire dorsal surface relatively level
3) Unwrap bone from gauze and place in tray, with the dorsal side up and the distal end on the towels

Setting up the Machine

1) Ensure that the scale portion of the Biodent machine is plugged in, as well as the 'head' portion (the part that the probes will attach to)
2) Open the Biodent program on the computer, and click that you wish to enter a new specimen. I recommend following a naming convention like: A14-3949L, for consistency. Make sure to click the single forward arrow to proceed and not the double arrows (which will use 'fast' settings, that are not correct)
3) Enter the user's name and proceed
4) Select the Horse protocol from the dropdown menu (this step is very important!)

5) On the parameters for quick viewing, it does not really matter what you select (as all parameters are saved), but I recommend initial indentation distance, total indentation distance, indentation distance increase, average creep and touch down distance. Proceed to start

Installing and 'Calibrating' the Probe

1) Take the probe out of its plastic holding tube. There are two parts to the probe: the actual indentation probe (longer, needle-like) and a reference probe (hollowed, syringe-like). Take the indentation probe and place it into the Biodent testing apparatus (there is a magnet that will hold it when the probe is in the correct position). Then, carefully slide the reference probe over the indentation probe and screw it in by rotating counter-clockwise
2) For future reference, counter-clockwise rotation should expose more of the probe and clockwise rotation, less of the probe. If this is incorrect notation for your reference plane, then adjust accordingly
3) Rotate the reference probe so that the indentation probe is exposed, but not extending past reference probe. *If the indentation probe extends past the reference probe, it can be very easily damaged on touchdown. Be careful!*
4) On the testing page, look on the left side under testing location and type in 'PMMA', and add the site
5) Place the block of PMMA on the scale portion of the device and hit the 'tare' button

6) Note that the reference load for the device is intended to be around 1300-1350. Lower than this will result in the device failing to achieve a desired indentation force, and the test will fail

7) Rotate the knob on the head portion of the testing device until the probe contacts the PMMA and creates a force of 1300-1350g. I would recommend closer to the higher end, as the material and the head will have some elasticity and the force will decrease over time slowly

8) Type in the code on the paper insert included with the probe in the bottom left of the testing screen

9) Click on the 'Tuning Mode' checkbox for this first test, then click "Run" (or the go arrow)

10) Pay attention to two things: the output graph and the TDD (Touchdown Distance) provided under the output graph. The hysteresis curve should end approximately at the same displacement (y-axis) as it started. The TDD should be between 150-200um. If it is less than this, it implies that the indentation probe is too close to the specimen, so rotate the reference probe clockwise

11) Keep tuning the probes until the TDD is in the desired range

12) After the final tuning, turn off tuning mode and take an actual test on the PMMA block

Testing the Bone Sample: Dorsal Sites

1) Place the instrument tray with bone now on the scale (remove the PMMA) and tare

2) Just like before, name the location on the left side (ex: proximal dorsal would be proxdors) and line up the probe
3) Ensure that the area to be tested is completely clear of periosteum, because the viscoelastic properties will cause erroneous readings
4) Take a reading as before, without being in tuning mode (the device has been tuned using the PMMA, so you should not tune the device again until using another bone)
5) Move either the tray or the probe (if using a 3D probe stand) approximately 1-2mm from the previous site
6) Take at a minimum two more readings, paying attention to the spread of the initial indentation distance and indentation distance increases. If the variance is large, then take as many is necessary to reduce this variance (typically 5 tests if unstable readings are obtained)
7) Continue testing all dorsal sites until complete
8) Spray sites every 15 – 20 minutes with BES or when the surface appears to dry if earlier than this

Testing the Bone Sample: Lateral or Medial Sites

1) Testing these sites are the same as the dorsal sites, however some initial prep is required
2) Rotate the bone so that the dorsal side is facing the side of the container (palmar facing inward)

3) Using the C-clamp, clamp the bone to the instrument tray so that it does not move during testing. A good spot is usually right above the distal condyles

4) Take readings as before

5) When done, click the check mark to complete the tests

Cleaning Up

1) Unscrew the reference probe first, then remove the indentation probe and place both back into their plastic container

2) Wipe all surfaces clean with ethanol to reduce contamination

Osteoprobe Protocol

Materials

- Periosteal elevator
- Scalpel
- Bone sample (thawed)
- BES (in squirt bottle)
- Osteoprobe indentation device
- Associated Osteoprobe computer
- Standing clamps
- Gauze
- PMMA block

- Animal hair electric razor
- A marking pen
- Tape measure

Procedure

Testing the Bone Sample: Skin-on

1) Prepare the bone sample by clamping the distal and proximal ends between the two standing clamps, dorsal-side up. These will secure the bone while indentation tests are performed
2) Shave the skin on the sample using an electric razor, particularly in sites that will be tested
3) Measure the bone length using the tape measure and mark using the marking pen the 25%, 50% and 75% lengths (that correspond to proximal, midshaft and distal). **This step is very important,** as the Osteoprobe is the first test conducted and thus all other tests will be performed at these same sites
4) Prepare the Osteoprobe computer program with the necessary information (name, date, etc.). For sample name, use the following convention: YYYY-MM-DD-Accession Number+Limb Side (L or R) + distance longitudinally (25, 50 or 75) + site (Lateral = L, Dorsolateral = DL, etc.) + skin status (ns or sk). An example would be 2016-01-07-A14-4991R25DLns. Make sure to update the variables within this naming if they are ever changed, as this data is automatically extracted using a custom MATLAB program!

5) When you have done all the necessary pre-tasks, the Osteoprobe will prompt you for readings. Carefully pierce the skin at one of the 12 sites with the Osteoprobe until the entire probe has entered

6) Preload the device normal to the site surface by pressing slowly into the bone. When the Osteoprobe detects a load of 10N, it will automatically perform the first indentation of 40N

7) Move the Osteoprobe under the skin approximately 1 – 2mm and take another reading, and repeat this until 10 good readings are taken. The Osteoprobe computer keeps track of the moving average of the indentations, so if a measure strays too far or seems erroneous, eliminate it by clicking on the point and take a replacement measurement. In all cases, make sure to take **ten 'good' measurements before proceeding!**

8) Once the ten measures are taken, click next and you will be asked to perform a calibration. Indent the provided block of PMMA normal to the surface just as with the bone tests for a total of five indentations and proceed

9) The Osteoprobe report will inform you as to whether (based on the standard deviation) the tests were 'Stable' or 'Unstable' – if the results are Unstable, it is recommended to re-do them

10) Repeat this process for all 12 sites, for the dorsal sites make sure to push the dorsal tendon out of the way to try and get as close to the dorsal surface as possible for dorsomedial and dorsolateral measures

Testing the Bone Sample: Skin Removed

1) This procedure is identical to the skin-on testing, with a few exceptions that will be listed here
2) Remove the skin using a scalpel blade or knife, being careful not to scrape the testing surfaces
3) Be sure to use the marking pen to label the tested 25%, 50% and 75% locations as before, as these will be used to directly identify tested locations for the Biodent and Raman spectroscopy modalities
4) Using a periosteal elevator or scalpel, remove a small portion of periosteum around each tested site prior to the normal operation of the Osteoprobe
5) Perform tests as before, ensuring that all 12 sites are tested prior to completion

Cleaning Up

1) Wrap the newly-tested bone in BES-soaked gauze and place in a labeled plastic bag. If no more tests are to be run, put the sample in the freezer until further testing is required
2) Wipe down surfaces with ethanol to prevent contamination

Raman Protocol

Materials:

- Periosteal elevator
- Scalpel
- Bone sample (thawed)
- BES (in squirt bottle)
- Silicon Dioxide calibration sample
- HR800 Raman Microspectrometer with Labspec 8
- Fiber optic light (or some other light source for the microscope)
- C-clamps (1 or 2)
- Instrument tray for holding sample
- Paper towels (3 or 4)
- Gauze

Procedure:

Calibration: Testing a Silicon Sample

1) The distinct fingerprint of silicon shows up at 520.7cm^{-1}, and is used as a calibrating value for the software. These next steps will ensure that the spectrometer is correctly picking up signal.
2) Open the laser shutter and using the camera, focus on the silicon sample with the laser and fiber optic light

3) Ensure that units are set to wavenumber, and that ‘Set units to pixels’ is deselected in the Instrument → Calibration menu

4) Put the plunger up and click ‘RTD Spectrum Acquisition’

5) Note that there are two peaks: one near 0, and one near 520cm^{-1}. The first signal is the Rayleigh scattered signal from the laser, which is unshifted. The second is the silicon peak, which has been shifted by Stokes scattering. This signal will be used to calibrate the software, and ***must be done every day!***

6) Zoom into the zero peak by dragging a box around the base. Right-click and choose “format and scale”, and freeze the axes. After calibrating the zero peak, unselect this option

7) In the calibration dialogue, adjust the ‘Zero’ value until the peak is over 0

8) Perform the same steps for the Silicon spectrum, trying to center the peak over 520.7cm^{-1}. In the case of the silicon peak, adjust the ‘Koeff’ value. I recommend only changing the last digit unless absolutely necessary, as it is very sensitive to changes

Obtaining a Bone Spectra: Preparation Stage

1) Wet paper towels and fold in-half twice (just dampened) – these will be used to prop the distal end of the bone, which serves two purposes. One, it provides friction to prevent the bone from sliding in the tray, and two, the distal end is slightly sloped, so it makes the entire dorsal surface relatively level

2) Unwrap bone from gauze and place in tray, with the dorsal side up and the distal end on the towels

3) Ensure the room is as dark as possible by closing the door to the microscope room

Obtaining a Bone Spectra: Dorsal Sites

1) Place the instrument tray with bone onto the scissor jack

2) Ensure that the area to be tested is completely clear of periosteum, and remove any excess using the periosteal elevator

3) With the plunger down and laser on, focus on the sample surface at one of the dorsal testing sites using the 50x objective lens. Ensure that the laser is as focused as possible

4) **If the laser loses focus rapidly, the bone is still moving – allow the bone to rest undisturbed for ten minutes!**

5) If good focus is acquired, take an extended range scan. The limits of the scan are 700 and 1800cm^{-1}, with 5 scans per region. The hole size should be 300µm and the slit should be 100µm. If absolutely necessary (for example, the Raman spectrometer is no longer reading properly) these can be adjusted, but they should be as consistent as possible!

6) Wait for the scan to complete, then take at a minimum two more readings. If the spectrum looks erroneous, then repeat the scan

7) If the scan is successful, perform ‘automatic’ baseline correction (this will use linear baseline correction with anywhere from 2 – 7 sites, and is used for consistency). Apply the ‘Standard’ denoise option to smooth the data and save it

as a .txt. In a folder with the accession number of the horse, use the location as the name and append a number for the repeat value (for example, the first distal dorsal measurement would be distdors1)

8) If the scan is unsuccessful due to spiking, re-run the scan
9) If the scan produces a fuzzy spectrum, scrape the bone surface lightly with a scalpel, taking care to spray the bone down afterwards
10) Test the remainder of the dorsal sites
11) Spray sites every 15 – 20 minutes with BES or when the surface appears to dry if earlier than this

Obtaining a Bone Spectra: Lateral or Medial Sites

1) Testing these sites are exactly the same as the dorsal sites, however some initial prep is required
2) Rotate the bone so that the dorsal side is facing the side of the container (palmar facing inward)
3) Using the C-clamp, clamp the bone to the instrument tray so that it does not move during testing. A good spot is usually right above the distal condyles
4) **I highly recommend waiting 10 minutes prior to attempting to focus as the bone will continue to move under the clamps!**
5) Take readings as in the previous section

Cleaning Up

1) Turn off the laser and fiber optic light

2) Wipe all surfaces clean with ethanol to reduce contamination

3) If bone is complete, return to freezer after wrapping with BES-soaked gauze

pQCT Protocol

Materials

- XCT3000 pQCT device with associated testing program
- Bone sample (frozen)
- ‘Cortical phantom’ and ‘Cone phantom’ for calibration

Procedure

Starting the program and calibration

1) Open the Animal CT program on the desktop
2) If you haven’t done a calibration scan since midnight of that day, the program will automatically prompt you to do these scans
3) Ensure that the proper holder for the two calibration samples is in place; if not, be sure to click “Yes, and Change Holder” when prompted. Secure the sample to the holder and begin each scan.
4) User input will be requested on one of the scans following a Scout View (SV) scan, simply press enter (the program will automatically find the correct location on the SV scan).

5) Ensure that the calibration results say something along the lines of “Sample is good” at the completion of the scan
6) When asked about saving and appending results, indicate yes, but do *not* print the results
7) Calibration should now be complete once both samples have been tested

Entering a patient and starting a scan

1) Find the enter new patient dialogue and press enter. On this screen, you need only fill out the name and birth sections. For this, you should use the accession number and limb side (ex: A14-394R) for the name, and the date of the scan for the birthdate
2) Press F4 and continue to the scan details page
3) For horse studies, press F6 and select the option pertaining to masks. Select either RMC3 0 25 etc. or LM3 0 25 etc. depending on which limbside it is and press enter
4) On this screen, fill in only the object length and do not change anything else (length is in mm, and can be either measured by hand or obtained from radiographs)
5) Press F4 and click change holder now – replace the calibration holder with the tester holder (a half circle) and put the testing tube through the machine
6) Place the specimen, in bag, dorsal side up with the proximal end facing the holder

7) Once you've changed the holder, proceed to the screen that asks the user to align the patient. Place the very end of the proximal side of the bone aligned with the red laser from the pQCT machine. This will align the bone with the distal carpals (assuming the proximal carpals have been removed prior). Start the SV scan
8) On the SV scan results, click on the start point of the MC3, *not the start or end points of the distal carpals!* There should be a gap on the SV with either side having bone – because the SV is taken from bottom to top, the top portion of bone is the proximal end of the MC3. Select this and proceed with the scan
9) The scan will take approximately 45 minutes, during which time you should leave the room
10) Once the scan is complete, it will automatically take the user back to the home page

Analyzing the scans

1) Go from the home page to the Analyze tab and select a patient. Proceed until you see slice scans. Navigate on the bottom options to Macro, and select MC3. When asked to proceed with the macro MC3, say yes
2) You will now draw areas of interest for each scan slice. Keeping the default name for each slide, the macro will ask you to make an ROC. Click okay, and use the free form lasso tool to draw around the MC3. Be sure not to include the splint bones, or the sesamoids if they haven't been removed prior. If you make a mistake, click cancel and click okay to drawing an ROC again. When you're done, click ok, and then click Done on the slices page. It will search through each

of the nine expected slices for the bone you just completed. Do this for all nine slices for each bone until you are not prompted to draw ROC's

3) The results are saved in a database file called MC3. The easiest way to find it is to search the computer for a file called MC3, and finding the most recently updated version